Systemic Human ILC Precursors Provide a Substrate for Tissue ILC Differentiation.

Ai Ing Li, Yan Li, Silvia Lopez-Lastra, Ralph Stadhouders, Franziska Paul, Armanda Casrouge, Nicolas Serafini, Anne Puel, Jacinta Bustamante, Laura Surace, et al.

▶ **To cite this version:**

Ai Ing Li, Yan Li, Silvia Lopez-Lastra, Ralph Stadhouders, Franziska Paul, et al.. Systemic Human ILC Precursors Provide a Substrate for Tissue ILC Differentiation.. Cell, 2017, 168 (6), pp.1086-1100.e10. 10.1016/j.cell.2017.02.021 . pasteur-01501939

HAL Id: pasteur-01501939

https://pasteur.hal.science/pasteur-01501939v1

Submitted on 18 May 2017

HAL is a multi-disciplinary open access archive for the deposit and dissemination of scientific research documents, whether they are published or not. The documents may come from teaching and research institutions in France or abroad, or from public or private research centers.

L'archive ouverte pluridisciplinaire **HAL**, est destinée au dépôt et à la diffusion de documents scientifiques de niveau recherche, publiés ou non, émanant des établissements d'enseignement et de recherche français ou étrangers, des laboratoires publics ou privés.

Distributed under a Creative Commons Attribution - NonCommercial - NoDerivatives 4.0 International License

Systemic human ILC precursors provide a substrate for tissue ILC differentiation

Ai Ing Lim[1,2,3], Yan Li[1,2], Silvia Lopez-Lastra[1,2,4], Ralph Stadhouders[5], Franziska Paul[6], Armanda Casrouge[1,2], Nicolas Serafini[1,2], Anne Puel[7,8], Jacinta Bustamante[7,8], Laura Surace[1,2], Guillemette Masse-Ranson[1,2], Eyal David[6], Helene Strick-Marchand[1,2], Lionel Le Bourhis[9], Roberto Cocchi[10], Davide Topazio[10], Paolo Graziano[10], Lucia Anna Muscarella[10], Lars Rogge[11], Xavier Norel[12], Jean-Michel Sallenave[3,13], Matthieu Allez[9,14], Thomas Graf[5], Rudi W. Hendriks[15], Jean-Laurent Casanova[7,8,16,17,18], Ido Amit[6], Hans Yssel[19] and James P. Di Santo[1,2,§].

[1]*Innate Immunity Unit, Institut Pasteur, 75724 Paris, France*

[2]*Inserm U1223, 75015 Paris, France*

[3]*Université Paris-Diderot, Sorbonne Paris Cité, 75205 Paris, France*

[4]*Université Paris-Sud, Paris-Saclay, 91405 Orsay, France*

[5]*Centre for Genomic Regulation, The Barcelona Institute of Science and Technology, 08003 Barcelona, Spain*

[6]*Department of Immunology, Weizmann Institute of Science, 76100 Rehovot, Israel*

[7]*Laboratory of Human Genetics of Infectious Diseases, Necker Branch, Inserm U1163, 75015 Paris, France*

[8]*Paris Descartes University, Imagine Institute, 75015 Paris, France*

[9]*Inserm U1160, Institut Universitaire d'Hématologie, Hôpital Saint-Louis, 75010 Paris, France*

[10]*Laboratory of Oncology, Scientific Institute for Research and Health Care "Casa Sollievo della Sofferenza", 71013 San Giovanni Rotondo, Italy*

[11]*Immunoregulation Unit, Institut Pasteur, 25 rue du Docteur Roux, 75724 Paris, France*

[12]*Inserm U1148, Laboratory for Vascular Translational Science (LVTS), CHU X. Bichat, 75877 Paris, France*

[13]*Inserm U1152, Faculté de Médicine site Bichat, Université Paris Diderot, Université Sorbonne Paris-Cité, 75018 Paris, France*

[14]*Gastroenterology Department, Hôpital Saint-Louis, AP-HP, 75010 Paris, France*

[15]*Department of Pulmonary Medicine, Erasmus MC, 3000 CA Rotterdam, Netherlands*

[16]*St. Giles Laboratory of Human Genetics of Infectious Diseases, Rockefeller Branch, The Rockefeller University, New York, NY 10065*

[17]*Howard Hughes Medical Institute, NY 10065*

[18]*Pediatric Hematology-Immunology Unit, Necker Hospital for Sick Children, 75015 Paris, France*

[19]*Inserm U1135, Centre d'Immunologie et des Maladies Infectieuses, 75013 Paris, France*

§ Lead contact to whom correspondence should be addressed:

Innate Immunity Unit

Institut Pasteur

25 rue du Docteur Roux

75724 Paris, France

Tel : + 33 1 45 68 86 96

Fax : + 33 1 40 61 35 10

Email : james.di-santo@pasteur.fr

Summary

Innate lymphoid cells (ILC) represent innate versions of T helper and cytotoxic T cells that differentiate from committed ILC precursors (ILCP). How ILCP give rise to mature tissue-resident ILC remains unclear. Here we identify circulating and tissue ILCP in humans that fail to express the transcription factors and cytokine outputs of mature ILCs but have these signature loci in an epigenetically poised configuration. Human ILCP robustly generate all ILC subsets *in vitro* and *in vivo*. While human ILCP express low levels of RAR related orphan receptor C (RORC) transcripts, these cells are found in RORC-deficient patients and retain potential for $EOMES^+$ NK cells, IFN-γ^+ ILC1, IL-13^+ ILC2 and for IL-22^+ but not for IL-$17A^+$ ILC3. Our results support a model of tissue ILC differentiation ('ILC-poiesis') whereby diverse ILC subsets are generated *in situ* from systemically distributed ILCP in response to local environmental signals.

Keywords: Innate lymphoid cells, development, lymphopoiesis, transcription factors, cytokines, cell fate, signaling

Introduction

Innate lymphoid cells (ILC) are a novel family of lymphoid effector cells that serve essential roles in the early immune response, comprising both 'cytotoxic' ILC (NK cells) and 'helper' ILC. The latter are characterized by CD127 expression and categorized as three groups based on transcription factors (TF) and cytokine outputs. Group 1 ILC (ILC1) express TBX21 (encoding T-BET) and produce T helper (T_H)1-associated cytokines IFN-γ and TNF-α. Group 2 ILC (ILC2) express GATA-3 and RORA and secrete T_H2-associated cytokines, IL-5 and IL-13. Group 3 ILC (ILC3) utilize RORC (encoding RORγt) to drive production of the T_H17-associated cytokines, IL-17 and/or IL-22 (Serafini et al., 2015; Spits et al., 2013). These different ILC subsets are found in diverse lymphoid and non-lymphoid tissues, and enriched at mucosal sites where they play essential roles in barrier function and innate immune defense (Artis and Spits, 2015; Eberl et al., 2015).

Human ILC subsets were first identified in secondary lymphoid tissues and subsequently reported in intestine, lung, liver and skin (Juelke and Romagnani, 2016). Two distinct populations of IFN-γ-producing ILC1 have been described. A T-BET$^+$ cell expressing high levels of CD127 and CD161 has been identified in tonsil and inflamed intestine (Bernink et al., 2013). In contrast, an intraepithelial ILC1 expressing NKp44 and CD103 but not CD127 resides at mucosal sites (Fuchs et al., 2013). Both these ILC1s produce IFN-γ in response to IL-12 but unlike NK cells they show minimal EOMES expression. Human GATA-3$^+$ ILC2 express the chemoattractant receptor CRTh2 as well as IL-25R and IL-33R (Mjösberg et al., 2011), are systemically distributed and produce IL-5 and IL-13 under physio- and pathological situations (Kim and Artis, 2015). Group 3 ILC include RORγt$^+$ fetal lymphoid tissue-inducer (LTi) cells in fetal lymph nodes and spleen (Cupedo et al., 2009) as well as adult lineage$^-$CD127$^+$CD117$^+$ cells found in tonsils, intestine, spleen, skin, lung, endometrium and decidua that produce IL-17A in response to IL-23 (Klose and Artis, 2016).

A subset of ILC3 express natural cytotoxicity receptors (NCR) and are enriched in IL-22-producing cells (Cella et al., 2009; Satoh-Takayama et al., 2008).

Murine ILC differentiate from hematopoietic stem cells (HSC) via lymphoid progenitors to yield diverse $ID2^+TCF\text{-}1^+PLZF^+$ ILC precursors (ILCP) in fetal liver (FL) and adult bone marrow (BM) (Constantinides et al., 2014; Yang et al., 2015). Several TF and signaling pathways regulate this process in mice (Serafini et al., 2015); in contrast, human ILC development is less well characterized (Juelke and Romagnani, 2016)). NK precursors (NKP) have been identified in FL, BM, cord blood (CB) and adult tonsil (Renoux et al., 2015), whereas committed ILC3 precursors (ILC3P) are found in tonsil and intestinal lamina propria but not peripheral blood (PB), thymus or BM (Montaldo et al., 2014). A recent study identified tonsillar human $ROR\gamma t^+$ ILCP that can develop into mature cytotoxic and helper ILC (Scoville et al., 2016). Interestingly, these human NKP, ILC3P and ILCP were $CD34^+$ and enriched in secondary lymphoid tissues but were rare or absent from the circulation. It was unclear how these $CD34^+$ hematopoietic precursors were developmentally related to mature tissue-resident ILC subsets.

In this report, we have extensively characterized the phenotypic, molecular and functional attributes of PB and tissue $CD117^+$ ILCs. This included an *in vitro* study of over 1300 ILC clonal cultures as well as an *in vivo* analysis using humanized mice. While ILCs with the $CD117^+$ phenotype were previously proposed to represent human ILC3 (Hazenberg and Spits, 2014), we find that PB $CD117^+$ cells are remarkably enriched in multi-potent and uni-potent ILC precursors (ILCP) that can give rise *in vitro* and *in vivo* to all known ILC subsets, including $EOMES^+$ NK cells. $CD117^+$ ILCP are found not only in the circulation, but also in tissues where they retain ILC multi-potency. Our identification of systemically distributed ILCP suggests a model whereby circulating and tissue ILCP provide a cellular substrate for ILC differentiation *in situ* in response to local environmental signals.

Results

Characterization of human peripheral blood CD117$^+$ ILC

Circulating ILC can be identified as a low frequency population (< 0.2% of total CD45$^+$ cells) within lineage$^-$CD7$^+$CD56$^-$CD127$^+$ peripheral blood (PB) cells of healthy individuals as well as patients suffering from diverse clinical syndromes ((Hazenberg and Spits, 2014; Munneke et al., 2014); Figure 1A and 1B). Further fractionation of PB ILCs into ILC1, ILC2 and ILC3 has been achieved using phenotypic markers, including CD161, CRTh2, CD117 and NKp44, that distinguish ILC subsets in fetal and adult tissues (Spits et al., 2013). Circulating ILCs include predominant CRTh2$^+$ ILC2 and a CD117$^+$ subset that lacks CRTh2 expression (Figure 1A and 1B). While CD117$^+$ cells are generally considered as circulating ILC3 (Hazenberg and Spits, 2014; Munneke et al., 2014), we found that PB CD117$^+$ ILC differ dramatically from gut CD117$^+$ ILC in that they lack protein expression of NKp44 and RORγt that identifies ILC3 (Figure 1C and S1A). Accordingly, PB CD117$^+$ ILC do not produce IL-17A or IL-22 after pharmacological stimulation, whereas gut CD117$^+$ cells abundantly produce these ILC3-associated cytokines (Figure 1D). Interestingly, circulating CD117$^+$ ILC express high levels of IL-1R1, CD45RA and are CD69$^-$, whereas gut-resident ILC3 are CD69$^+$ but IL-1R1$^-$ and CD45RA$^-$ (Figure 1C and S1B). These observations suggest that PB CD117$^+$ ILC differ from *bona fide* ILC3.

PB CD117$^+$ ILC also do not express proteins for TF that characterize other known mature ILC subsets, including T-BET or EOMES (Figure 1C), although a fraction expressed PLZF (Figure S1B). Accordingly, PB CD117$^+$ ILC failed to express markers associated with NK cells, ILC1 and ILC2, such as CD94, CD244, CRTh2 (Figure S1B) and did not produce IFN-γ or IL-13 after stimulation with pharmacological activators (Figure 1D). Taken together, these results suggest that PB CD117$^+$ ILC may represent an unusual ILC subset.

Transcription and chromatin landscapes of CD117$^+$ ILC reveal an ILC precursor profile

In order to further understand the identity of PB CD117$^+$ ILC, we profiled the transcriptomic and epigenetic landscapes of highly purified circulating CD117$^+$ ILC compared to CD34$^+$ HSC (Figure 2A). We performed chromatin immunoprecipitation followed by high-throughput sequencing using transposase-mediated tagmentation (ChIPm-Seq; (Schmidl et al., 2015). To expose common and unique epigenetic features of CD34$^+$ HSC and CD117$^+$ ILC, we mapped histone H3 lysine 4 di-methyl modifications (H3K4Me2), which marks both active and poised gene regulatory elements (GRE) (Koche et al., 2011). We identified around 18,000 and 35,000 GRE in CD117$^+$ ILC and CD34$^+$ HSC respectively (Figure 2B; Table S1), the majority of which were located in introns and intergenic regions (Figure S2A). A significant number of H3K4Me2$^+$ GRE were shared between the two cell types: 89% of GRE identified in CD117$^+$ ILC showed similar enrichment in HSC and were associated with 13159 genes of which many encoded housekeeping functions. Nevertheless, 11% of H3K4Me2$^+$ GRE detected in CD117$^+$ ILC were absent in CD34$^+$ HSC, potentially regulating 2283 genes. Pathway analysis of these genes revealed a strong enrichment for immune system and lymphocyte related processes. Conversely, GRE only active in CD34$^+$ HSC were located near genes involved in more general pathways important for hematopoiesis, hemostasis, and platelet activation (Figure 2C).

We compared the transcriptome of CD117$^+$ ILC and CD34$^+$ HSC. Clear differences in gene expression profiles emerged, with a large cluster of 1540 genes expressed at substantially higher levels in CD117$^+$ ILC (Figure 2D; Table S2) including many genes linked to the lymphoid lineage (*IKZF1*, *CD2, CD7 and IL7R*). In contrast, CD34$^+$ HSC cells highly expressed genes involved in the broader development of diverse hematopoietic lineages, including *ID1, GATA1, GATA2* and *MYB* (Figure 2D and S2B) as well as cytokine receptors for myeloid lineages (*CSF3R, CSF2RB, FLT3*). Compared to HSC, CD117$^+$ ILC express high

levels of TF that have been shown to be essential for murine ILC development, including *ID2, GATA3, TOX* and *TCF7*. We did not detect transcripts characteristic of T and B cells development, such as *RAG1, RAG2, EBF1, CD3E, BCL11A* or *LMO2* in CD117$^+$ ILC although some of these genes are expressed by CD34$^+$ HSC (Figure S2B).

As both transcriptomic and epigenetic analyses of CD117$^+$ ILC identified strong lymphoid signatures, we intersected these datasets in order to gain insights into the developmental status and potential of CD117$^+$ ILC. A substantial proportion (26%) of the genes most highly expressed in CD117$^+$ ILC were located in the direct vicinity of a CD117$^+$ ILC-specific GRE (Figure 2E and Table S3). These included many transcription factors previously implicated in mouse ILC development, including *ID2, GATA3, ETS1, TOX, TCF7, RORA, ZBTB16* and *NOTCH1* (Figure 2E and S2A) – consistent with the commitment of CD117$^+$ ILC to the innate lymphoid fate. In contrast, we did not detect notable expression levels for TF (*EOMES, TBX21, RORC*), cytokine receptors (*CCR6*, *IL1RL1*, *IL23R*) or signature cytokines (*IFNG, IL13, IL5, IL22, IL17A*) that are abundantly expressed by mature ILCs (Koues et al., 2016). However, many of these mature ILC identity genes were already marked with H3K4Me2, demonstrating that they may reside in a poised state (Figure 2F and S2B). Together, these analyses suggest that CD117$^+$ ILC represent lymphoid-biased progenitors reminiscent of multi-potent ILCP carrying a TF profile with key mature ILC signature genes in an epigenetically poised state.

Peripheral blood CD117$^+$ ILC include multi-potent ILC precursors (ILCP)

In order to assess the hematopoietic potential of circulating CD117$^+$ ILC, we cultured these cells in the presence of various cytokines. As CD117$^+$ ILC express CD25, CD127 and IL-1R1 (Figures 1A, 1C and S1B), we added IL-2, IL-7 and/or IL-1β to these cultures. While bulk cultures of CD117$^+$ ILC minimally expanded in the presence of IL-2 and IL-7, robust

proliferation was observed when cells IL-1β was added to the cultures (Figure S3A). The overall cell yield was reduced by more than 100-fold in the absence of any one of these cytokines (Figure S3A). Cultured cells did not harbor B ($CD19^+$) or T ($CD3^+CD5^+$) cells but comprised a pure population of $CD7^+$ cells that were $CD161^+$ and expressed variable levels of CD117 and CD25 (Figure 3A). Remarkably, expanded cells included some $EOMES^+CD94^+$ NK cells as well as the three canonical ILC groups: IFN-γ^+ ILC1, IL-13^+ ILC2 and $NKp44^+$IL-$17A^+$IL-22^+ ILC3 (Figure 3A and S3B). ILC1 ($NKp44^-$, $CD25^-$), ILC2 ($NKp44^-CD25^+$) and ILC3 ($NKp44^+CD25^-$) subsets expressed signature TF (Figure S3C). While the additional presence of cytokines that can drive ILC1/NK (IL-12, -18), ILC2 (IL-25, -33) or ILC3 (IL-23) development did not further increase cell yield over that obtained with IL-2, IL-7 and IL-1β (Figure 3B and S3A), the addition of IL-12 clearly promoted the development of $EOMES^+CD94^+$ IFN-γ-producing NK cells and IL-23 was critical for IL-17A-producing-ILC3 (Figures 3A and S3D). These results not only define a cytokine millieu that supports multi-lineage ILC and NK cell generation (IL-2, IL-7, IL-1β, IL-23) but also suggest that the PB $CD117^+$ ILCs harbor multi-potent ILC precursors (ILCP).

We further characterized circulating $CD117^+$ ILCP using a modified stromal cell-based culture system that is permissive for B cell, T cell and myeloid cell development (Figure 3C, (Mohtashami et al., 2010)). Moreover, this system can extensively expand human NK cells and ILC subsets at the clonal level with minimal plasticity (Lim et al., 2016). We analyzed progeny of single PB $CD117^+$ ILC cultured on OP9 and OP9-DL4 to identify $EOMES^+$ NK cells and ILC subsets expressing signature TF and producing IFN-γ, IL-13, IL-17A and/or IL-22 (Figure 3D, S3E). Our analysis of over 340 clonal PB cultures allows several points to be made. First, PB $CD117^+$ ILC represent a heterogeneous population of uni-potent and multi-potent ILCP. Roughly half of the cultures derived from single $CD117^+$ ILC generated a single ILC1, ILC2 or ILC3 subset and therefore represent lineage-restricted ILCP,

whereas the remainder are multi-potent ILCP that can give rise to 2 or more separate Lin$^-$ CD7$^+$ ILC lineages (Figure 3E; Table S4). B cell and T cell potential was not observed. Second, within the multi-potent ILCP population, a substantial fraction (between 9-17%) are able to generate all three ILC subsets and likely represent immature uncommitted ILCP. Moreover, clonal IFN-γ^+ cultures also comprise EOMES$^+$ NK cells demonstrating that some PB ILCP have the potential to generate both 'helper' and 'cytotoxic' ILC lineages at the single cell level. Third, a subset of Lin$^-$CD7$^+$ ILC clones failed to produce any cytokine tested (Figure 3E; Table S4). As these clones maintained high level of CD117 but lacked other ILC markers, they may represent ILCP that have not further differentiated (Figure S3F). Fourth, Notch signals clearly influence the cell fate potential of CD117$^+$ ILCP as multi-potentiality and development of ILC3-containing cells was enhanced on OP9-DL4 (Figure 3E; Table S4). Together, these data identify PB CD117$^+$ ILC as a circulating pool of partially committed ILC progenitors. The comparison of bulk and clonal assays clearly demonstrate the importance of the single cell approach to define heterogeneity of CD117$^+$ ILC cell fate potential and to establish functional multi-potency.

Circulating CD117$^+$ ILCP have multi-ILC potential in vivo in humanized mice

We next assessed the *in vivo* potential of PB CD117$^+$ ILCP. Severely immunodeficient mouse strains engrafted with human CD34$^+$ HSC progenitors generate human lymphoid (B, T, NK) and myeloid (DC, macrophage, neutrophils) cell subsets (reviewed in (Rongvaux et al., 2013)). We used BALB/c *Rag2*$^{-/-}$*Il2rg*$^{-/-}$*Sirpa*^{NOD} (BRGS) mice that are permissive for robust multi-lineage human hematopoietic cell engraftment, including NK cells (Legrand et al., 2011). Human PB CD34$^+$ HSC and CD117$^+$ ILCP were transferred to newborn BRGS mice; cytokine supplementation (human IL-2, IL-7, IL-1β, IL-23) was provided and mice were analyzed 4 weeks later (Figure 4A). BRGS mice engrafted with human CD34$^+$ HSC

developed CD19$^+$ B cells and CD14/CD33$^+$ myeloid cells in the bone marrow, while CD3/CD5$^+$ T cells and Lin$^-$ CD7$^+$ cells were detected in the gut (Figure 4B). These include mature ILC3 as previously described (Zhang et al., 2015). In contrast, BRGS mice receiving PB CD117$^+$ ILCP developed Lin$^-$CD7$^+$ cells but no myeloid cells, B cells or T cells. Human CD45$^+$ progeny from transferred CD117$^+$ ILCP were detected in multiple organs, including the spleen, lung, gut and liver (Figure 4C). At each of these tissue sites, EOMES$^+$ NK cells as well as diverse CD127$^+$ ILC subsets could be identified that expressed RORγt and GATA-3 proteins and produced IFN-γ, IL-13, IL-17A and/or IL-22 *ex vivo* upon stimulation (Figure 4C). These results demonstrate that PB CD117$^+$ cells comprise committed ILCP having the capacity to generate all known ILC subsets and NK cells *in vivo*.

Human CD117$^+$ ILCP develop from CD34$^+$ HSC in vivo

We next interrogated the developmental relationship between CD34$^+$ HSC and CD117$^+$ ILCP in 'humanized' BRGS mice (Figure 5A). Mice engrafted with CD34$^+$ HSC harbored human CD45$^+$ cells in the BM, lung, liver and spleen that included a variety of lineage$^+$ T, B, myeloid cells as well as mature NK cells, ILC1 and ILC3 (Figure 5B, data not shown) as previously described (Legrand et al., 2011; Zhang et al., 2015). Moreover, within the subset of Lin$^-$CD7$^+$ cells, a clearly defined subpopulation of CD127$^+$CD117$^+$ cells could be discerned in multiple tissues that lacked T-BET and EOMES expression (Figure 5B and 5C). These included CD127$^+$CD117$^+$ cells that expressed low levels of GATA-3 and RORγt and were NKp44$^-$ (Figure 5D) and therefore resembled PB CD117$^+$ ILCP. *Ex vivo* stimulation failed to elicit cytokine production from CD127$^+$CD117$^+$ cells (Figure 5E). We sorted these cells and cultured them in the presence of IL-2, IL-7, IL-1β and IL-23. Expanded cells contained subsets able to produce IFN-γ, IL-13, IL-17A and IL-22 (Figure 5E) thereby

confirming the presence of human ILCP. These results demonstrate that fetal liver $CD34^+$ HSC can give rise to $CD117^+$ ILCP *in vivo*.

Human $CD117^+$ ILCP are present in fetal liver, cord blood and adult lung

We next assessed the stage of development when human $CD117^+$ ILCP arise. Fetal liver (FL) harbors several immature hematopoietic precursor populations (Rollini et al., 2007) and is proposed as a site for the development of lymphoid tissue inducer cells in the mouse (Cherrier et al., 2012). Lin^-CD127^+ ILC within FL contain a predominant $CD117^+$ subset (Figure S4A). Interestingly, these cells express RORγt at levels exceeding their peripheral blood counterparts (Figure 1C and S4A) and moreover express CCR6, Neuropilin-1 (NRP-1) but not NKp44 (Figure S4A and S4B). Despite these differences, FL $CD117^+$ ILC did not produce significant amounts of IL-17A or IL-22 after stimulation (Figure S4C) suggesting that they were not fully mature ILC3. Nevertheless, when FL $CD117^+$ ILC were expanded *in vitro*, IL-17A-producing ILC3 were abundantly generated. Moreover, $IL17A^+$ ILC3 developed on stromal cells lacking the Notch ligand DL4 suggesting that Notch engagement is not necessary for this process (Figure 6A). Interestingly, bulk cultures of FL $CD117^+$ ILC also contain IL-13- and IFN-γ-producing cells, although at lower frequency. Clonal analysis revealed that FL $CD117^+$ ILC harbor a high proportion of ILC3 committed progenitors. Still, a substantial fraction of multi-potent ILCP can be revealed in the presence of Notch ligands (Figure 6B and 6C; Table S5).

We next characterized $CD117^+$ ILC from human CB. Like their PB counterparts, CB $CD117^+$ ILC lacked NKp44, CCR6 and NRP-1 and were $CD45RA^+$ (Figure S4A and S4B). Moreover, CB $CD117^+$ ILC failed to express RORγt and T-BET but were GATA-3^{lo}, thus resembling PB ILCP (Figure 1C and S4A). Like PB $CD117^+$ ILC, CB $CD117^+$ ILC did not produce cytokines *ex vivo* after stimulation (Figure S4C). However, culture of CB $CD117^+$

ILC generated IFN-γ^+ ILC1, IL-13$^+$ ILC2 and IL-17A$^+$ or IL-22$^+$ ILC3 (Figure 6D). No T, B or myeloid cells were detected in cultures of CB CD117$^+$ ILC (data not shown). Further clonal analysis revealed that CB CD117$^+$ ILC harbored a diverse mix of uni-potent and multi-potent ILCP (Figure 6E and 6F; Table S5). Unlike FL CD117$^+$ ILC, CB CD117$^+$ ILC were not biased towards ILC3-committed progenitors, but more closely resembled PB CD117$^+$ ILCP. As for ILCP from PB or FL, Notch stimulation resulted in an enhanced frequency of multi-potent ILCP (especially those having the potential for IL-17A$^+$ and IL-22$^+$ ILC3) and reduced the frequency of cytokine$^-$ ILC clones.

We also examined the phenotype and potential of CD117$^+$ ILC from adult lung tissue. Lung CD117$^+$ ILC harbored discrete populations of NKp44$^+$ and RORγt$^+$ ILC but were largely CD45A$^-$ (Figure S4A and S4B). Bulk cultures of lung CD117$^+$ ILC generated diverse cytokine-producing ILC subsets and EOMES$^+$ NK cells (Figure 6G); further analysis using clonal assays defined the NKp44$^-$ fraction of lung CD117$^+$ ILC as a mixture of uni-potent and multi-potent ILCP (Figure 6H and 6I; Table S5). These results demonstrate that a variety of ILCP, including multi-potent progenitors, are present in human mucosal tissues.

ILC precursors reside within secondary lymphoid tissues

As human secondary lymphoid tissues (lymph nodes, tonsils) harbor diverse ILC subsets and their precursors, we further characterized tonsillar CD117$^+$ ILCP and assessed their cell fate potential. CD117$^+$ ILC from pediatric tonsils harbor a predominant NKp44$^+$ ILC3 subset that can be stimulated to produce IL-17A and IL-22 (Hoorweg et al., 2012). This population also appears to have extensive functional plasticity as stimulation (using IL-1β, IL-12, IL-23) modifies their cytokine production (Bernink et al., 2015; Bernink et al., 2013; Cella et al., 2010). Within tonsillar CD117$^+$ ILC, we found that NKp44$^-$ cells were CD45RA$^+$ and NRP-1$^-$, while NKp44$^+$ cells were CD45RA$^-$ and NRP-1$^+$ (Figure S4B). These findings

suggest that NKp44^{+} ILC3 are more mature (Bernink et al., 2015). However, cytokine production profiles were different in bulk cultures from tonsillar NKp44^{-} versus NKp44^{+} CD117^{+} ILC (Figure 6J and 6M). In particular, IFN-γ^{+} cells and IL-13^{+} cells were more obvious in cultures derived from NKp44^{-} cells, especially on OP9 stroma (Figure 6J).

In order to better understand the relationship between NKp44^{-} and NKp44^{+} CD117^{+} ILC, we generated clones from both subsets and analyzed their cytokine-production potential. Striking differences were observed. Clones derived from NKp44^{+} CD117^{+} ILC were highly enriched ILC3 producing IL-17A and/or IL-22 (Figure 6N and 6O; Table S5). A fraction of clones co-expressed IFN-γ (14%) that likely represent 'plastic' ILC3 that may up-regulate T-BET as previously shown (Bernink et al., 2015). In contrast, clones derived from NKp44^{-} CD117^{+} ILC were quite heterogeneous with cells producing not only IL-22 and/or IL-17A but also abundant single IFN-γ^{+} clones as well as single IL-13^{+} clones (Figure 6K and 6L; Table S5) that were not detected from NKp44^{+} CD117^{+} ILC (Figure 6N and 6O; Table S5). The presence of IFN-γ^{+} ILC1 clones was unexpected given previous reports that tonsillar CD127^{+} ILC1 differentiate into IL-22 producing ILC3 in the presence of IL-2, IL-23 and IL-1β (Bernink et al., 2015). Lastly, multi-potent ILCP giving rise to three ILC subsets were only found in NKp44^{-} CD117^{+} ILC. Taken together, these results suggest that tonsillar CD117^{+} harbor NKp44^{-} ILCP as well as NKp44^{+} ILC3.

RORC-deficient patients harbor ILCP but fail to generate IL-17A^{+} ILC3

A committed ILCP in human secondary lymphoid tissue with a CD34^{+}CD45RA^{+}CD117^{+} phenotype was shown to highly express the TF RORC (Scoville et al., 2016). In order to address whether RORC is required for generation of human CD117^{+} ILCP, we studied blood ILC in RORC-deficient patients. RORC deficiency in humans is associated with mycobacterial disease and mucocutaneous candidiasis and a defect in Th1 and

Th17 differentiation (Okada et al., 2015). $CD117^+$ ILC are reduced in patients with RORC deficiency, while $CD56^{bright}$ and $CD56^{dim}$ NK cells were unaffected (Figure 7A and 7B). In contrast, ILC1 were present and the percentage of ILC2 from total ILC was significantly increased in the absence of RORC (Figure 7B). Sorted $CD117^+$ ILC from control and RORC-deficient patients were cultured as described above. Robust growth of Lin^-CD7^+ cells was observed with no significant difference between WT and RORC-deficient cells. We identified diverse cytokine producing cells in these cultures, including those producing IFN-γ, IL-13 or IL-22, however, there was a total absence of IL-17A-producing ILC3 (Figure 7C). Development of $EOMES^+IFN\text{-}\gamma^+$ NK cells was not affected by the absence of RORC. These results demonstrate that RORC is not required for the development of NK cells, ILC1, ILC2 or $IL\text{-}22^+$ ILC3 but is essential for the generation of $IL\text{-}17A^+$ ILC3 from ILCP in humans.

Discussion

In this report, we identify and characterize human ILC precursors (ILCP) as a subset of $Lin^{-}CD7^{+}CD127^{+}CD117^{+}$ cells in cord and adult blood as well as fetal liver and several adult tissues. Human ILCP give rise to all mature ILC subsets that are capable of producing a range of cytokines (IFN-γ, IL-13, IL-17A, IL-22) after *in vitro* culture in an appropriate cytokine environment or after transfer *in vivo* to immunodeficient mice. Human ILCP also generate $EOMES^{+}$ NK cells demonstrating their potential for both cytokine-producing and cytotoxic ILCs. This is the first evidence for a circulating ILCP in any species and further demonstrate the broad systemic distribution of ILCP within human lymphoid and non-lymphoid tissues including mucosal sites (Figure S5).

The identification of human ILCP was possible thanks to a robust OP9 stromal cell-based assay that could assess ILC potential at the single cell level. With this approach, we analyzed over 1300 ILC clonal cultures and identified uni-potent ILCP that could give rise to IFN-γ^{+} ILC1, IL-13^{+} ILC2 or IL-$17A^{+}$ and/or IL-22^{+} ILC3 as well as multi-potent human ILCP that could generate two or more ILC subsets. We further demonstrate that human $CD34^{+}$ HSC can develop *in vivo* into $CD117^{+}$ cells that harbored ILCP with multi-lineage ILC potential. Both *in vitro* and *in vivo* ILCP differentiation to more mature ILC subsets required exogenous cytokines, especially IL-2, IL-7 and IL-1β; as such, availability of these factors may condition ILCP differentiation during immune responses. Our results suggest a model for human ILCP development whereby pluripotent $CD34^{+}$ HSC progressively differentiate into multi-potent ILCP (with the $CD34^{-}CD7^{+}CD127^{+}CD117^{+}CD45RA^{+}$ phenotype) with potential for ILC1, ILC2, ILC3 and $EOMES^{+}$ NK cells. Both $CD34^{+}$ HSC and multi-potent ILCP are present in fetal liver suggesting that this tissue is permissive for this transition. While previously described human tonsillar $CD34^{+}CD117^{+}CD45RA^{+}$ ILCP (Scoville et al., 2016) may represent an intermediate in this pathway, the absence of these

cells in BM, as well as cord and adult blood (Scoville et al., 2016) suggests that $CD34^+$ ILCP arise locally. The circulating and tissue $CD34^-$ ILCP that we describe also harbor cells with more restricted uni-potent ILC. While we have not identified a marker that allows distinction between multi-potent and uni-potent ILCP, we assume that they retain a precursor-product relationship.

Transcriptomic and epigenomic analysis of circulating human ILCP revealed a signature consistent with a partial specification to the ILC lineage. TF known to be critical for ILC development in mice (including *TCF7*, *TOX, ID2, ZBTB16* and *GATA*3; (Constantinides et al., 2014; Klose et al., 2014; Seehus et al., 2015; Serafini et al., 2014; Yagi et al., 2014; Yang et al., 2015)) were clearly up-regulated in ILCP compared to circulating HSC. In contrast, signatures of early B and T lymphopoiesis were not obvious, consistent with the inability of ILCP to generate adaptive lymphocytes *in vitro* or *in vivo*. Previous studies have carefully analyzed the epigenomic and transcriptional landscape of human mucosal ILC subsets (Koues et al., 2016). These studies identified distinct transcriptional signatures for ILC1, ILC3 and conventional NK cells as well as shared gene circuitry associated with ILC lineage differentiation under the control of defined 'super enhancers' (Koues et al., 2016). In contrast, we find that the ILC group-defining TFs (*BCL11B, TBX21, EOMES, RORC*) and effector molecules (*IFNG, IL13, IL17A, IL22, IL26*) identified by Koues et al. were not expressed by circulating ILCP (Table S2) suggesting commitment to ILC1, ILC2 or ILC3 had not yet occurred. Interestingly, the loci encoding these factors were still 'poised' as evidenced by abundant H3K4Me2 epigenetic modifications consistent with establishing of ILC 'regulomes' at an early developmental stage (Shih et al., 2016). This chromatin landscape likely facilitates rapid generation of differentiated ILC subsets following cytokine-driven expansion (Lara-Astiaso et al., 2014; Zook et al., 2016).

Mature ILCs and fully differentiated T_H cells possess striking similarities (Spits et al., 2013). T_H cells arise following antigen activation of naive T cells within specialized zones of secondary lymphoid tissues. While the analogous sites and structures that promote ILC differentiation are not known, it is interesting to consider circulating and tissue ILCP as the functional innate counterpart of naive T cells. Both naïve T cells and ILCP are $CD45RA^+$ and $CD69^-$ suggestive of a resting state. Human and mouse ILCP clearly demonstrate the potential for further differentiation to all known ILC subsets and lack expression of the signature TF that drive mature ILC effector functions. As such, ILCP resemble naïve T cells that can differentiate to diverse T helper subsets under appropriate environmental signals. Nevertheless, human ILCP have signature TF in a poised state which contrasts with the situation in naïve T cells where these loci are actively repressed (Shih et al., 2016). Moreover, ILCP expand extensively in the presence of cytokines, whereas naïve T cell homeostasis is primarily maintained through cytokine-driven survival (Marrack and Kappler, 2004). Taken together, ILCP appear to have some properties in common with naïve T cells, although a number of important differences exist that are consistent with their designation as immature progenitors.

While uni-potent and multi-potent ILCP were identified in every human tissue sample tested, there were clearly differences in the relative proportions of ILCP that were uni- or multi-potent. It is therefore likely that each tissue harbors a unique ILCP 'repertoire' conditioned by environmental signals. One may include Notch signals that appear to influence ILCP multi-potency and ILC3 fate, particularly in the fetal liver. It is remarkable that other uni-potent ILCP were rarely detected in this organ, suggesting that at this stage of fetal development, the microenvironment may deliver signals that strongly polarize ILCP towards ILC3. These results corroborate earlier findings in the mouse (Cherrier et al., 2012). Notch-mediated signaling has been proposed to play a role in directing lymphoid cell fate decisions,

promoting the development of T-lineage primed precursors as well as modifying ILCP homeostasis (Chea et al., 2016; Dallas et al., 2005). Soluble factors are also likely to be involved in ILCP 'repertoires' as these cells express several cytokine receptors (IL-1R, IL-2R, IL-18R) that allow them to sense tissue inflammation and stress.

Regulation of TF expression dictates ILC fate as well as function. Signature TF have been identified for ILC subsets that regulate their differentiation at the level of surface phenotype and effector outputs (Serafini et al., 2015). The TF RORC helps define the ILC3 subset and is required for ILC3 development and maintenance in mice (Satoh-Takayama et al., 2008; Sawa et al., 2010). RORC is expressed by human ILC3 and in committed ILC3P (Montaldo et al., 2014). The recent report that all human ILC subsets express RORC (Scoville et al., 2016) suggested a broader role for this TF in human ILC differentiation. By analyzing blood from RORC null patients, we could show that RORC was not required for global ILC differentiation in humans, but rather was critical for IL-17 production by the ILC3 subset. ILCP in RORC-deficient patients retained the capacity to generate other cytokine-producing ILC and NK cell subsets. It is noteworthy that IL-22$^+$ ILC3 developed in a RORC-independent fashion, suggesting compensatory pathways for these cells in humans.

We have previously shown that OP9 stroma minimizes human ILC2 plasticity (Lim et al., 2016) and extend this observation by showing that in this culture system the vast majority of NKp44$^+$ ILC3 clones retain their functional attributes with little plasticity towards the ILC1 phenotype. Moreover, previous reports proposed that ILC1 clones rapidly differentiate towards an ILC3 fate in the presence of IL-1β (Bernink et al., 2015), whereas we found that ILC1 clones on OP9 stroma (containing IL-1β) retained their IFN-γ signature. As such, our culture system appears useful to assess signals that promote 'primary' ILC fate from ILCP.

Finally, our identification of circulating and tissue-resident human ILCP suggests a concept of 'ILC-poiesis' in which ILC differentiation can occur 'on demand' in any tissue and

at any age. A recent study using parabiosis in mice has proposed that ILCs are long-lived tissue-resident cells that do not recirculate under steady-state and some inflammatory conditions (Gasteiger et al., 2015). In contrast, the half-life of several mucosal ILC subsets in the mouse is on the order of weeks, suggesting that these cells must be renewed (Sawa et al., 2010). The discovery of a circulating ILCP provides a mechanism to replenish tissue ILCs in response to steady-state losses and in the context of infection and inflammation.

Author Contributions

Conceptualization, A.I.L. and J.P.D.; Methodology, A.I.L., Y.L., R.S., F.P., H.S-M., H.Y.; Software, R.S., F.P., E.D.; Formal Analysis, A.I.L., S.L-L., R.S., F.P., E.D.; Investigation: A.I.L., Y.L. S.L-L, R.S., F.P., A.C., N.S., L.S., G.M-R.; Resources: A.P., J.B., L.L.B, R.C., D.T., P.G., L.A.M., L.R., X.N., J-M.S., M.A., T.G., R.H., J-L.C., I.A.; Writing, A.I.L., R.S., J.P.D.; Funding Acquisition, J.P.D.; Supervision, J.P.D.

Acknowledgements

We thank all the members of Innate Immunity Unit for helpful discussions, the Centre de Recherche Translationnelle, F. Pala and O. Fiquet (Institut Pasteur), and A. Sparaneo (Casa Sollievo della Sofferenza) for technical assistance. AIL is a scholar in Pasteur-Paris University (PPU) International PhD program and supported by FP7 under grant agreement n°317057 (HOMIN) and the Fondation ARC. RS was supported by EMBO (ALTF 1201-2014) and Marie Curie (H2020-MSCA-IF-2014). Supported by grants from the Institut Pasteur, Inserm, Laboratoire d'Excellence REVIVE, ANR and FP7 under grant agreements n°305578 (PathCO) and n°317057 (HOMIN). James Di Santo is a founder of AXENIS (Paris, France) and a member of its advisory board. The other authors declare no conflict of interest.

References

Artis, D., and Spits, H. (2015). The biology of innate lymphoid cells. Nature *517*, 293-301.

Bernink, J.H., Krabbendam, L., Germar, K., de Jong, E., Gronke, K., Kofoed-Nielsen, M., Munneke, J.M., Hazenberg, M.D., Villaudy, J., Buskens, C.J., *et al.* (2015). Interleukin-12 and -23 Control Plasticity of CD127(+) Group 1 and Group 3 Innate Lymphoid Cells in the Intestinal Lamina Propria. Immunity *43*, 146-160.

Bernink, J.H., Peters, C.P., Munneke, M., te Velde, A.A., Meijer, S.L., Weijer, K., Hreggvidsdottir, H.S., Heinsbroek, S.E., Legrand, N., Buskens, C.J., *et al.* (2013). Human type 1 innate lymphoid cells accumulate in inflamed mucosal tissues. Nat Immunol *14*, 221-229.

Cella, M., Fuchs, A., Vermi, W., Facchetti, F., Otero, K., Lennerz, J.K., Doherty, J.M., Mills, J.C., and Colonna, M. (2009). A human natural killer cell subset provides an innate source of IL-22 for mucosal immunity. Nature *457*, 722-725.

Cella, M., Otero, K., and Colonna, M. (2010). Expansion of human NK-22 cells with IL-7, IL-2, and IL-1beta reveals intrinsic functional plasticity. Proc Natl Acad Sci U S A *107*, 10961-10966.

Chea, S., Schmutz, S., Berthault, C., Perchet, T., Petit, M., Burlen-Defranoux, O., Goldrath, A.W., Rodewald, H.R., Cumano, A., and Golub, R. (2016). Single-Cell Gene Expression Analyses Reveal Heterogeneous Responsiveness of Fetal Innate Lymphoid Progenitors to Notch Signaling. Cell Rep *14*, 1500-1516.

Cherrier, M., Sawa, S., and Eberl, G. (2012). Notch, Id2, and RORγt sequentially orchestrate the fetal development of lymphoid tissue inducer cells. J Exp Med *209*, 729-740.

Constantinides, M.G., McDonald, B.D., Verhoef, P.A., and Bendelac, A. (2014). A committed precursor to innate lymphoid cells. Nature *508*, 397-401.

Cupedo, T., Crellin, N.K., Papazian, N., Rombouts, E.J., Weijer, K., Grogan, J.L., Fibbe, W.E., Cornelissen, J.J., and Spits, H. (2009). Human fetal lymphoid tissue-inducer cells are interleukin 17-producing precursors to RORC+ CD127+ natural killer-like cells. Nat Immunol *10*, 66-74.

Dallas, M.H., Varnum-Finney, B., Delaney, C., Kato, K., and Bernstein, I.D. (2005). Density of the Notch ligand Delta1 determines generation of B and T cell precursors from hematopoietic stem cells. J Exp Med *201*, 1361-1366.

Eberl, G., Colonna, M., Di Santo, J.P., and McKenzie, A.N. (2015). Innate lymphoid cells. Innate lymphoid cells: a new paradigm in immunology. Science *348*, aaa6566.

Fuchs, A., Vermi, W., Lee, J.S., Lonardi, S., Gilfillan, S., Newberry, R.D., Cella, M., and Colonna, M. (2013). Intraepithelial type 1 innate lymphoid cells are a unique subset of IL-12- and IL-15-responsive IFN-γ-producing cells. Immunity *38*, 769-781.

Gasteiger, G., Fan, X., Dikiy, S., Lee, S.Y., and Rudensky, A.Y. (2015). Tissue residency of innate lymphoid cells in lymphoid and nonlymphoid organs. Science *350*, 981-985.

Hazenberg, M.D., and Spits, H. (2014). Human innate lymphoid cells. Blood *124*, 700-709.

Heinz, S., Benner, C., Spann, N., Bertolino, E., Lin, Y.C., Laslo, P., Cheng, J.X., Murre, C., Singh, H., and Glass, C.K. (2010). Simple combinations of lineage-determining transcription factors prime cis-regulatory elements required for macrophage and B cell identities. Mol Cell *38*, 576-589.

Hoorweg, K., Peters, C.P., Cornelissen, F., Aparicio-Domingo, P., Papazian, N., Kazemier, G., Mjösberg, J.M., Spits, H., and Cupedo, T. (2012). Functional Differences between Human NKp44(-) and NKp44(+) RORC(+) Innate Lymphoid Cells. Front Immunol *3*, 72.

Jaitin, D.A., Kenigsberg, E., Keren-Shaul, H., Elefant, N., Paul, F., Zaretsky, I., Mildner, A., Cohen, N., Jung, S., Tanay, A., *et al.* (2014). Massively parallel single-cell RNA-seq for marker-free decomposition of tissues into cell types. Science *343*, 776-779.

Juelke, K., and Romagnani, C. (2016). Differentiation of human innate lymphoid cells (ILCs). Curr Opin Immunol *38*, 75-85.
Kim, B.S., and Artis, D. (2015). Group 2 innate lymphoid cells in health and disease. Cold Spring Harb Perspect Biol *7*.
Klose, C.S., and Artis, D. (2016). Innate lymphoid cells as regulators of immunity, inflammation and tissue homeostasis. Nat Immunol *17*, 765-774.
Klose, C.S., Flach, M., Möhle, L., Rogell, L., Hoyler, T., Ebert, K., Fabiunke, C., Pfeifer, D., Sexl, V., Fonseca-Pereira, D.*, et al.* (2014). Differentiation of type 1 ILCs from a common progenitor to all helper-like innate lymphoid cell lineages. Cell *157*, 340-356.
Koche, R.P., Smith, Z.D., Adli, M., Gu, H., Ku, M., Gnirke, A., Bernstein, B.E., and Meissner, A. (2011). Reprogramming factor expression initiates widespread targeted chromatin remodeling. Cell Stem Cell *8*, 96-105.
Koues, O.I., Collins, P.L., Cella, M., Robinette, M.L., Porter, S.I., Pyfrom, S.C., Payton, J.E., Colonna, M., and Oltz, E.M. (2016). Distinct Gene Regulatory Pathways for Human Innate versus Adaptive Lymphoid Cells. Cell *165*, 1134-1146.
Langmead, B., and Salzberg, S.L. (2012). Fast gapped-read alignment with Bowtie 2. Nat Methods *9*, 357-359.
Lara-Astiaso, D., Weiner, A., Lorenzo-Vivas, E., Zaretsky, I., Jaitin, D.A., David, E., Keren-Shaul, H., Mildner, A., Winter, D., Jung, S.*, et al.* (2014). Immunogenetics. Chromatin state dynamics during blood formation. Science *345*, 943-949.
Legrand, N., Huntington, N.D., Nagasawa, M., Bakker, A.Q., Schotte, R., Strick-Marchand, H., de Geus, S.J., Pouw, S.M., Böhne, M., Voordouw, A.*, et al.* (2011). Functional CD47/signal regulatory protein alpha (SIRP(alpha)) interaction is required for optimal human T- and natural killer- (NK) cell homeostasis in vivo. Proc Natl Acad Sci U S A *108*, 13224-13229.
Lim, A.I., Menegatti, S., Bustamante, J., Le Bourhis, L., Allez, M., Rogge, L., Casanova, J.L., Yssel, H., and Di Santo, J.P. (2016). IL-12 drives functional plasticity of human group 2 innate lymphoid cells. J Exp Med *213*, 569-583.
Marrack, P., and Kappler, J. (2004). Control of T cell viability. Annu Rev Immunol *22*, 765-787.
McLean, C.Y., Bristor, D., Hiller, M., Clarke, S.L., Schaar, B.T., Lowe, C.B., Wenger, A.M., and Bejerano, G. (2010). GREAT improves functional interpretation of cis-regulatory regions. Nat Biotechnol *28*, 495-501.
Mjösberg, J.M., Trifari, S., Crellin, N.K., Peters, C.P., van Drunen, C.M., Piet, B., Fokkens, W.J., Cupedo, T., and Spits, H. (2011). Human IL-25- and IL-33-responsive type 2 innate lymphoid cells are defined by expression of CRTH2 and CD161. Nat Immunol *12*, 1055-1062.
Mohtashami, M., Shah, D.K., Nakase, H., Kianizad, K., Petrie, H.T., and Zúñiga-Pflücker, J.C. (2010). Direct comparison of Dll1- and Dll4-mediated Notch activation levels shows differential lymphomyeloid lineage commitment outcomes. J Immunol *185*, 867-876.
Montaldo, E., Teixeira-Alves, L.G., Glatzer, T., Durek, P., Stervbo, U., Hamann, W., Babic, M., Paclik, D., Stölzel, K., Gröne, J.*, et al.* (2014). Human RORγt(+)CD34(+) cells are lineage-specified progenitors of group 3 RORγt(+) innate lymphoid cells. Immunity *41*, 988-1000.
Munneke, J.M., Björklund, A.T., Mjösberg, J.M., Garming-Legert, K., Bernink, J.H., Blom, B., Huisman, C., van Oers, M.H., Spits, H., Malmberg, K.J.*, et al.* (2014). Activated innate lymphoid cells are associated with a reduced susceptibility to graft-versus-host disease. Blood *124*, 812-821.
Okada, S., Markle, J.G., Deenick, E.K., Mele, F., Averbuch, D., Lagos, M., Alzahrani, M., Al-Muhsen, S., Halwani, R., Ma, C.S.*, et al.* (2015). IMMUNODEFICIENCIES. Impairment

of immunity to Candida and Mycobacterium in humans with bi-allelic RORC mutations. Science *349*, 606-613.
Quinlan, A.R., and Hall, I.M. (2010). BEDTools: a flexible suite of utilities for comparing genomic features. Bioinformatics *26*, 841-842.
Rollini, P., Faes-Van't Hull, E., Kaiser, S., Kapp, U., and Leyvraz, S. (2007). Phenotypic and functional analysis of human fetal liver hematopoietic stem cells in culture. Stem Cells Dev *16*, 281-296.
Rongvaux, A., Takizawa, H., Strowig, T., Willinger, T., Eynon, E.E., Flavell, R.A., and Manz M.G. (2013). Human hemato-lymphoid system mice: current use and future potential for medicine. Annu Rev Immunol. *31*, 635-674.
Saldanha, A.J. (2004). Java Treeview--extensible visualization of microarray data. Bioinformatics *20*, 3246-3248.
Satoh-Takayama, N., Vosshenrich, C.A., Lesjean-Pottier, S., Sawa, S., Lochner, M., Rattis, F., Mention, J.J., Thiam, K., Cerf-Bensussan, N., Mandelboim, O.*, et al.* (2008). Microbial flora drives interleukin 22 production in intestinal NKp46+ cells that provide innate mucosal immune defense. Immunity *29*, 958-970.
Sawa, S., Cherrier, M., Lochner, M., Satoh-Takayama, N., Fehling, H.J., Langa, F., Di Santo, J.P., and Eberl, G. (2010). Lineage relationship analysis of RORgammat+ innate lymphoid cells. Science *330*, 665-669.
Schmidl, C., Rendeiro, A.F., Sheffield, N.C., and Bock, C. (2015). ChIPmentation: fast, robust, low-input ChIP-seq for histones and transcription factors. Nat Methods *12*, 963-965.
Scoville, S.D., Mundy-Bosse, B.L., Zhang, M.H., Chen, L., Zhang, X., Keller, K.A., Hughes, T., Cheng, S., Bergin, S.M., Mao, H.C.*, et al.* (2016). A Progenitor Cell Expressing Transcription Factor RORγt Generates All Human Innate Lymphoid Cell Subsets. Immunity *44*, 1140-1150.
Seehus, C.R., Aliahmad, P., de la Torre, B., Iliev, I.D., Spurka, L., Funari, V.A., and Kaye, J. (2015). The development of innate lymphoid cells requires TOX-dependent generation of a common innate lymphoid cell progenitor. Nat Immunol *16*, 599-608.
Serafini, N., Klein Wolterink, R.G., Satoh-Takayama, N., Xu, W., Vosshenrich, C.A., Hendriks, R.W., and Di Santo, J.P. (2014). Gata3 drives development of RORγt+ group 3 innate lymphoid cells. J Exp Med *211*, 199-208.
Serafini, N., Vosshenrich, C.A., and Di Santo, J.P. (2015). Transcriptional regulation of innate lymphoid cell fate. Nat Rev Immunol *15*, 415-428.
Shih, H.Y., Sciumè, G., Mikami, Y., Guo, L., Sun, H.W., Brooks, S.R., Urban, J.F., Davis, F.P., Kanno, Y., and O'Shea, J.J. (2016). Developmental Acquisition of Regulomes Underlies Innate Lymphoid Cell Functionality. Cell *165*, 1120-1133.
Spits, H., Artis, D., Colonna, M., Diefenbach, A., Di Santo, J.P., Eberl, G., Koyasu, S., Locksley, R.M., McKenzie, A.N., Mebius, R.E.*, et al.* (2013). Innate lymphoid cells--a proposal for uniform nomenclature. Nat Rev Immunol *13*, 145-149.
Yagi, R., Zhong, C., Northrup, D.L., Yu, F., Bouladoux, N., Spencer, S., Hu, G., Barron, L., Sharma, S., Nakayama, T.*, et al.* (2014). The transcription factor GATA3 is critical for the development of all IL-7Rα-expressing innate lymphoid cells. Immunity *40*, 378-388.
Yang, Q., Li, F., Harly, C., Xing, S., Ye, L., Xia, X., Wang, H., Wang, X., Yu, S., Zhou, X.*, et al.* (2015). TCF-1 upregulation identifies early innate lymphoid progenitors in the bone marrow. Nat Immunol *16*, 1044-1050.
Zhang, Z., Cheng, L., Zhao, J., Li, G., Zhang, L., Chen, W., Nie, W., Reszka-Blanco, N.J., Wang, F.S., and Su, L. (2015). Plasmacytoid dendritic cells promote HIV-1-induced group 3 innate lymphoid cell depletion. J Clin Invest *125*, 3692-3703.

Zook, E.C., Ramirez, K., Guo, X., van der Voort, G., Sigvardsson, M., Svensson, E.C., Fu, Y.X., and Kee, B.L. (2016). The ETS1 transcription factor is required for the development and cytokine-induced expansion of ILC2. J Exp Med *213*, 687-696.

Main Figure Legends

Figure 1. Characterization of peripheral blood CD117$^+$ILC

(A) Gating strategy for FACS analysis of human PB ILC. Total ILC were gated on viable CD45$^+$ Lin$^-$ (CD3$^-$CD4$^-$CD5$^-$TCRαβ$^-$TCRγδ$^-$CD14$^-$CD19$^-$) CD7$^+$CD127$^+$ cells (red). NK cells are identified by CD56^{dim} (grey), ILC2 are marked by CRTh2$^+$ cells (green) and CD117$^+$ ILC are gated on CRTh2$^-$CD117$^+$ population (blue). (B) Percentage of total ILC from viable CD45$^+$CD117$^+$ ILC from total ILC of healthy adult donors in PB. Results from 27 healthy individuals (Median). (C) Expression of surface phenotypes (NKp44, IL1R1 and CD69) and intracellular transcription factors (EOMES, T-BET, GATA-3 and RORγt) of PB CD117$^+$ ILC and gut CD117$^+$NKp44$^{+/-}$ ILC. (D) Functional profiles (IFN-γ, IL-13, IL-22 and IL-17A) of PB CD117$^+$ ILC and gut CD117$^+$NKp44$^{+/-}$ ILC in response to 3 h PMA/iono stimulation. Data representative of at least 3 individuals analyzed from at least 3 independent experiments. See also Figure S1.

Figure 2. The transcriptional signature and chromatin landscape of CD117$^+$ ILC

(A) Schematic for RNA-Seq and ChIPm-Seq analyses. (B) Heat map depicting normalized ChIPm-Seq signal showed H3K4me2 intensity of 36449 high-confidence regulatory region, of which 1989 were unique to CD117$^+$ ILC. Venn diagram shows the overlap between three categories of H3KMe2$^+$ regions ('CD34$^+$ HSC-specific'; 'CD117$^+$ ILC-specific' and 'shared'). (C) Heat map of significantly enriched molecular pathways associated with genes near GREs uniquely identified in CD117$^+$ ILC (blue) or CD34$^+$ HSC (orange). (D) Heat map with clustering of differentially expressed genes between CD117$^+$ ILC (blue) and CD34$^+$ HSC

(orange) as detected by RNA-Seq. (E) Overlap of the 1540 genes most highly expressed by CD117$^+$ ILC and 2283 genes associated with 'CD117$^+$ ILC-specific' H3KMe2$^+$ GREs. Selected genes essential for ILC development are highlighted. (F) RNA-Seq reads and corresponding H3K4Me2 traces are shown for selected loci. See also Figure S2, Tables S1-3.

Figure 3. Cloning reveal multi-ILC lineage potential of CD117$^+$ ILC *in vitro*

(A) FACS analysis of bulk cultured CD117$^+$ ILC for surface phenotypes, intracellular EOMES and cytokine expression after 3h PMA/ionomycin stimulation to identify NK cells (EOMES$^+$ cells), ILC1 (IFN-γ$^+$ cells), ILC2 (IL-13$^+$) and ILC3 (IL-22$^+$ and/or IL-17A$^+$). (B) Expansion of bulk cultured CD117$^+$ ILC (10 days) in stromal cell-free conditions with cytokines (20 ng/ml each). Results from four independent donors; ns, $p>0.05$; **, $p<0.01$; ****, $p<0.0001$ using paired Student's t test compared to IL-2, IL-7 only condition (Median). (C) Schematic diagram and morphology of CD117$^+$ ILC-OP9 stromal co-culture system. (D) Single PB CD117$^+$ ILC were cultured on OP9 or OP9-DL4 stromal cells for 14-18 days. Cells were stimulated with PMA/iono 3h before cytokine analysis. IL-17A and IL-22 producing cells were analyzed after gating on cells not expressing IFN-γ or IL-13. Positive clones were considered when at least 100 viable human CD45$^+$ cells were detected by FACS. Presence of an ILC subset was scored when more than 5% of corresponding cytokine was detected in total viable CD45 cells. (E) Pie chart depicting all possible ILC combinations detected. Frequency of each single or multi ILC differentiation among total positive wells. Data summarized from four independent experiments with one donor each. See also Figure S3 and Table S4.

Figure 4. CD117$^+$ ILC effectively give rise to multi-ILC lineage *in vivo*

(A) Schematic diagram of *in vivo* transfer experiment. (B-C) Newborn BRGS mice were injected with PB $CD117^+$ ILC or $CD34^+$ HSC and analyzed 4 weeks later. (B) FACS analysis for lymphocytes and myeloid surface markers gated on viable human $CD45^+$ cells from bone marrow and gut. (C) ILC analysis within viable human $CD45^+$ cell using CD127, NKp44 and CD117 expression, intracellular TF (EOMES, GATA-3 and RORγt) and intracellular cytokines (IFN-γ, IL-13, IL-22 and IL-17A) production in lung, gut, liver and spleen of BRGS mice transferred with $CD117^+$ ILC. Representative data of at least 4 mice in each group from 3 independent experiments.

Figure 5. Human ILCP accumulate in human immune system (HIS) mice

(A) Schematic diagram of generation of HIS mice. Fetal liver $CD34^+CD38^-$ HSC were intrahepatically injected into newborn BRGS mice. Mice were analyzed 8 to 9 weeks later. (B) Representative FACS analysis of human ILCP ($Lin^-CD7^+CD127^+CD117^+$) in spleen, BM, lung and liver of HIS mice. (C) Percentage of ILCP from total human $CD45^+$ in spleen, BM, lung and liver of HIS mice (Median). (D) FACS analysis of surface phenotypes and transcription factors profiles of ILCP and NK cells from spleen of HIS mice. (E) Cytokine production of splenic $CD117^+$ ILC pre- and post-culture on OP9-DL4 with IL-2, IL-7, IL-1β, and IL-23 for 10 days. Cytokine production was analyzed after 3 h of PMA/iono stimulation. Representative data of 8 mice from at least 3 independent experiments.

Figure 6. *In vitro* bulk and clonal assay of $CD117^+$ ILC from lymphoid and non-lymphoid organs

Bulk (100-300 cells) or single $CD117^+$ $NKp44^{+/-}$ $CD117^+$ ILC from different organs were FACS sorted into 96 well round bottom plate pre-seeded with OP9 or OP9-DL4 and supplied with IL-2, IL-7, IL-1β and IL-23 (20 ng/ml each). Intracellular cytokine production in respond

to 3h PMA/iono stimulation was performed to identify ILC1 (IFN-γ^+), ILC2 (IL-13^+) and ILC3 (IL-22^+ and/or IL-$17A^+$) after 8-10 days bulk culture (A, D, G, J, M) or 14-18 days single cell culture (B-C, E-F, H-I, K-L, N-O). Representative FACS analysis of bulk cultured $CD117^+NKp44^-$ ILC isolated from (A) FL, (D) CB, (G) lung, (J) tonsil and $CD117^+NKp44^+$ from (M) tonsil. Pie chart depicting all possible ILC combinations after clonal expansion of $CD117^+NKp44^-$ ILC from (B-C) FL, (E-F) CB, (H-I) lung, (K-L) tonsil and (M-N) $CD117^+$ $NKp44^+$ from tonsil on OP9 and OP9-DL4. Data summarized from at least 2 independent experiments with one donor each. See also Figure S4.

Figure 7. Development potential of ILCP from RORC$^{-/-}$ patients

(A) FACS analysis of peripheral blood ILC subsets from healthy and $RORC^{-/-}$ patient samples. (B) Percentage of NK^{dim} and NK^{bright} from viable $CD45^+$ cells, ILC1, ILC2 and ILCP from total ILC of PB of healthy and $RORC^{-/-}$ patients. Result from 22 healthy donors and 2 $RORC^{-/-}$ patients. ns, $p>0.05$; *, $p<0.05$; **, $p<0.01$ using unpaired Student's t test (Median) (C) ILCP from healthy donor or $RORC^{-/-}$ patients were cultured on OP9-DL4 with IL-2, IL-7, IL-1β and IL-23 for 8 days prior to analysis.

Supplementary Figure Legends

Figure S1. CD117$^+$ ILC gating strategy, Related to Figure 1

(A) FACS analysis of ILCs from human peripheral blood and gut. CD117$^+$ ILC were gated on lymphoid size, singlet and viable CD45$^+$Lin$^-$CD7$^+$CD127$^+$CRTh2$^-$CD117$^+$ population. (B) Protein staining for surface receptors and intracellular PLZF in blood CD117$^+$ ILC (blue) and NK cells (grey).

Figure S2. Transcriptional and epigenetics signature of PB CD117$^+$ ILC, Related to Figure 2

(A) Annotation of H3K4Me2$^+$ regions as defined by their overlap with known genomic features. (B) Comparative transcriptional and epigenetics profiles of CD117$^+$ ILC and CD34$^+$ HSC for selective loci. Bar graphs show gene expression values identified by RNA-Seq from CD117$^+$ ILC (blue) and CD34$^+$ HSC (orange) (n=4, error bars denote SEM). Adjacent genome browser display normalized H3K4Me2 ChIPm-Seq signal in CD117$^+$ ILC (blue) or CD34$^+$ HSC (orange). Arrowheads mark regions of CD117$^+$ ILC-specific H3K4Me2 enrichment.

Figure S3. Cytokines environment dictate progeny of CD117$^+$ ILC, Related to Figure 3

(A) Fold expansion of bulk cultured PB CD117$^+$ ILC in cytokines (20 ng/ml each) for 10 days. (B) Cytokine production from *in vitro* expanded PB CD117$^+$ ILC after stimulation. (C) Surface phenotype and TF expression in expanded PB CD117$^+$ ILC. (D) Cytokines (IFN-γ, IL-13, IL-22 and IL-17A) production in response to 3h PMA/iono stimulation using different culture conditions. (E) Surface phenotype and TF expression of representative ILC1, ILC2

and ILC3 clones. (F) Surface phenotype, TF and cytokine production in PMA/iono stimulated 'cytokine negative' clones.

Figure S4. Gating strategy and characteristic of CD117$^+$ ILC from fetal liver, cord blood, lung and tonsil, Related to Figure 6

(A) Gating strategy for FACS analysis to identify CD117$^+$ ILC from fetal liver, cord blood, lung and tonsil. Surface expression for CRTh2 and NKp44, intracellular TF (RORγt, GATA-3 and T-BET) was compared between CD117$^+$NKp44$^-$ ILC (solid blue), CD117$^+$ NKp44$^+$ (dashed blue), CRTh2$^+$ ILC2 (green) and CD56$^+$ NK cells (grey). (B) Surface phenotypes of CD117$^+$NKp44$^-$ ILC (solid blue), CD117$^+$NKp44$^+$ (dashed blue), CRTh2$^+$ ILC2 (green) and CD56$^+$ NK cells (grey) from FL, CB, lung and tonsil. (C) Functional profiles of CD117$^+$ ILC (blue), and CD56$^+$ NK cells (grey) from FL, CB, lung and tonsil in response to 3 h PMA/iono stimulation.

Figure S5. Model for Human 'ILC-poiesis'

Human ILCP (Lin$^-$CD127$^+$CD117$^+$CD45RA$^+$IL1R1$^+$) within fetal and adult tissues as well as in the circulation can be detected that have potential for all ILC subsets and NK cells.

Supplementary Table Legends

Table S1. GRE specific for $CD117^+$ ILC and $CD34^+$ HSC are listed. Fraction of reads in peaks (FRIP) and percentage of duplication metrics for $CD117^+$ ILC and $CD34^+$ HSC are indicated; Related to Figure 2B

Table S2. RNA-Seq analysis with fold change and p value of differentially express genes between $CD117^+$ ILC and $CD34^+$ HSC, Related to Figure 2D

Table S3. Gene lists of active loci in circulating human ILCP, Related to Figure 2E

Table S4. Number of clones detected for all possible ILC combination from 340 $CD117^+$ ILC clones co-culture with OP9 or OP9-DL4 stroma cells, Related to Figure 3E

Table S5. Number of clones detected for all possible ILC combination from $CD117^+NKp44^{+/—}$ ILC clones from different tissues co-culture with OP9 or OP9-DL4 stroma cells, Related to Figure 6

STAR Methods

Contact for reagent and resources sharing

Further information may be directed to the corresponding author (james.di-santo@pasteur.fr).

Experimental model and subject details

Human blood and tissues samples

Blood samples from healthy donors were obtained from Establissement Français du Sang (EFS, Paris). Blood samples from patients with *RORC* mutation have been previously reported (Okada et al., 2015) including P2 from Kindred A (homozygous for S38L/38L isoform 1 or S17L/S17L isoform 2) and P6 from Kindred C (homozygous for Q441* isoform 1 or Q420* isoform 2). Fetal liver with gestational age ranging from 14 to 20 weeks were obtained from Advanced Bioscience Resources Inc. following approval of an institutional medical ethical committee at Institut Pasteur and the French Ministry of Education and Research (IF-20080451). Umbilical cord blood was collected from normal deliveries. Tonsils were obtained from pediatric patients undergoing routine tonsillectomy (Scientific Institute for Research and Health Care "Casa Sollievo della Sofferenza"). Lung and colon samples were obtained from adenocarcinoma and colon cancer patients, respectively undergoing therapeutic resection (Dr. X. Norel and J.-M. Sallenave, Hôpital Bichat; Dr. M Allez, Hôpital Saint Louis). Informed consent was obtained from all patients and included protocols approved by the institutional review boards of Necker Medical School, Paris Descartes University, Hôpital Bichat, Hôpital Saint Louis, Assistance Publique - Hôpital de Paris.

In vivo analysis using human immune system (HIS) mice model

BALB/c *Rag2*$^{-/-}$*Il2rg*$^{-/-}$*Sirpa*^{NOD} (BRGS) mice have been described (Legrand et al., 2011) and were maintained in isolators at Institut Pasteur. CD34^{+} HSC or CD117^{+} ILC were sorted from peripheral blood of healthy donors using a FACS Aria. Fetal liver CD34^{+}

HSC were isolated using CD34 Microbead Kit (Miltenyi). For *in vivo* transfer experiment, 1-3 x 10^5 $CD117^+$ ILC or $CD34^+$ HSC were intrahepatically injected into sublethal irradiated (3Gy) new born (3-7 days-old) BRGS mice together with 0.3 μg of IL-2 and IL-7 (Miltenyi). Mice received IL-2, IL-7, IL-1β, IL-23, IL-25 and IL-33 (0.3 μg each) by intraperitoneal injection weekly and were analyzed four weeks post-transplantation. For generation of HIS mice, 2 x 10^5 fetal liver-derived $CD34^+$ $CD38^-$ HSC were intrahepatically injected into sublethal irradiated (3Gy) new born (3-7 days-old) BRGS mice. Mice were sacrificed 8-9 weeks post-injection. Experiments were approved by ethical committee at Institut Pasteur and validated by French Ministry of Education and Research (MENESR#02162.02).

Method details

Cell isolation from blood, tonsil, gut, fetal liver and lung

Human peripheral blood mononuclear cells (PBMC) from CB and PB were isolated by Ficoll-Paque (GE Healthcare) density gradient centrifugation. Single cell suspension from fetal liver and tonsil was achieved by mechanical disruption through 70-μm filters. Lung and intestine samples were minced and digested with Liberase TL (25 μg/ml; Roche) and DNase I (50 μg/ml; Sigma-Aldrich) for 45min in 37°C shaking incubator. Digested tissues were passed through 70-μm filters. Lymphocytes from liver, lung and gut were isolated by Ficoll-Paque density gradient centrifugation.

FACS analysis and cell sorting

For FACS analysis, cells were first stained with Flexible Viability Dye eFluor 506 (eBioscience) for 10 min following by 20 min surface antibodies staining with Brilliant Stained Buffer (BD) on ice. For experiment involving intracellular TF staining, cells were fixed, permeabilized and stained using Foxp3/Transcription Factor Staining Buffer Kit (eBioscience). For intracellular cytokines staining, cells were stimulated with PMA (10ng/ml;

Sigma) plus Ionomycin (1μg/ml; Sigma) in the presence of Golgi Plug (BD) for 3 h in 37°C incubator. Cells were fixed, permeabilized and stained by Cytofix/Cytoperm Kit (BD). Samples were acquired on LSRFortessa (BD) and analyzed by FlowJ10 (Tree Star).

For cell sorting from healthy PB, PBMC were first depleted of T cell, B cell, pDC and monocytes by labeling with biotin-conjugated anti-CD3, anti-CD4, anti-CD19, anti-CD14, anti-CD123 followed by anti-biotin microbeads (Miltenyi) according to manufacturer's instructions. Sorting from CB and tissues were performed without lineage depletion. Bulk populations were sorted to a purity ≥ 99% or as single cell index sorting (both using FACSAria II; BD).

Bulk RNA isolation, library construction, sequencing and analysis

10^3 cells from each population were FACS sorted directly into 50 μl of lysis/binding buffer (Life Technologies). mRNA was captured with 15 μl Dynabeads oligo(dT) (Life Technologies), washed according to manufacturers' instructions and eluted at 85°C with 6 μl of 10mM Tris-HCl (pH7.5). We used a derivation of MARS-Seq as described (Jaitin et al., 2014), developed for single-cell RNA-Seq to produce expression libraries of two replicates per population. Libraries were sequenced at an average depth of 5 million reads per library on the Ilumina NextSeq and aligned to the human reference genome (hg19). Reads were mapped using hisat (version 0.1.6); duplicate reads were filtered if they had identical UMIs. Expression levels were calculated and normalized to the total number of reads using HOMER software (http://homer.salk.edu).

Chromatin immunoprecipitation and sequencing (Chip-Seq) using ChipMentation

FACS sorted cells (20-50K) were immediately crosslinked in PBS containing 1% formaldehyde (Sigma) for 10 min at room temperature for ChIP-Seq analysis. Crosslinking was quenched by adding glycine (0.125M final concentration) followed by 5 min incubation

at room temperature. Cells were placed on ice, washed with PBS and snap-frozen for storage at -80°C. Pellets were processed in parallel to minimize technical variation. Cells were resuspended in 100µl sonication buffer (1% SDS, 10mM EDTA, 50mM Tris-HCl pH8 and 1x EDTA-free complete protease inhibitors; Roche) and transferred to a 0.65ml Bioruptor sonication tube (Diagenode). After 15 min incubation on ice, cells were sonicated for 30 cycles (30 sec ON - 30 sec OFF) using a Bioruptor Pico sonicator (Diagenode) to shear chromatin down to ±250 bp fragments. Chromatin was equilibrated by adding 900µl 10x ChIP dilution buffer (0.01% SDS, 1.1% Triton X-100, 1.2mM EDTA, 16.7mM Tris-HCl pH8, 167mM NaCl) and incubated overnight at 4°C with 1µl of H3K4Me2-specific antibody (ab32356, Abcam) or normal rabbit IgG as a negative control (sc-2027, Santa Cruz). In addition, 20µl of protein A Dynabeads (Thermo Fisher Scientific) per IP were blocked in PBS containing 0.1% BSA (Sigma) by incubation overnight at 4°C. The next day, beads were resuspended in the original volume with ChIP dilution buffer and added to the chromatin extracts. After 2 hours of incubation at 4°C, beads were collected and washed with Low Salt buffer (0.1% SDS, 1% Triton X-100, 2mM EDTA, 20mM Tris-HCl pH8, 150mM NaCl), High Salt buffer (0.1% SDS, 1% Triton X-100, 2mM EDTA, 20mM Tris-HCl pH8, 500mM NaCl) and LiCl buffer (10mM Tris-HCl pH8, 1mM EDTA, 250mM LiCl, 0.5% NP-40, 0.5% deoxycholic acid). Chromatin-antibody immobilized on magnetic beads were then subjected to tagmentation as recently described (Schmidl et al., 2015). Eluted DNA was purified using MinElute spin columns (Qiagen) and amplified for 8-12 cycles using Nextera PCR primers. Libraries were purified using dual (0.5x-2.0x) SPRI Ampure XP beads (Beckman Coulter), pooled (up to 10 per sequencing run) and sequenced on a NextSeq500 (Illumina) running a single-read 75bp protocol.

ChIP-Seq data processing, analysis and visualization

Reads were demultiplexed using BaseSpace (Illumina) and aligned to the mouse genome (mm10 build) using Bowtie (Langmead and Salzberg, 2012) with standard settings, removing reads that could not be uniquely mapped. Indexed and sorted bam files were parsed to HOMER (Heinz et al., 2010) for further analysis. Tag directories were generated for each sample with removal of duplicate reads (-tbp 1 option). BedGraph files displaying normalized counts (reads per million) were generated for direct visualization in the UCSC Genome Browser (https://genome.ucsc.edu/) using the makeUCSCfile HOMER script. H3K4Me2 enriched regions were identified using HOMER findPeaks with -region -size 1000 -minDist 2500 options. Overlapping and non-overlapping regions between two samples were identified using the intersect function of BEDTools (Quinlan and Hall, 2010) or the HOMER mergePeaks script (-d given option) requiring a minimal overlap of 1bp. Sets of cell type-specific H3K4Me2+ regions were visualized as heatmaps with Java TreeView (Saldanha, 2004). Regions/peaks were assigned to putative target genes GREAT (McLean et al., 2010). GREAT was subsequently used to calculate enrichments of these genes for known pathway signatures using the whole genome as background. Fraction of reads in peaks (FRIP) and percentage of duplication metrics are included in Table S1.

Bulk and single cell culture

All *in vitro* culture experiments were performed in Yssel's medium (18432890) supplemented with 2% human AB serum (EFS). 2-3 x 10^3 stromal cells were pre-seeded in 96-well round bottom plates one night before culture. For bulk culture, 100-300 FACS sorted cell were plated on the stromal cells. For cloning experiment, cells were index-sorted directly into the 96-well plates pre-seeded with stromal cells. Cytokines IL-2, IL-7 (20 ng/ml each, Miltenyi), IL-12, IL-18, IL-25, IL-33, IL-1β, IL-23 (20 ng/ml each, R&D) were provided in various combinations as indicated. For bulk culture, fresh cytokines and medium were

replenish every 5 days and analyzed after 10 days expansion. For cloning experiment, cytokines and medium were replenished every 7 days and analyzed after 14-18 days of culture.

Quantification and statistical analysis

Data are represented as Median unless specified. The sample size for each experiment and the replicate number of experiments are included in the figure legends.

Data and software availability

Data resources

The accession number for the RNA-Seq and ChIPm-Seq analysis have been deposited in the NCBI Gene Expression Omnibus under accession numbers GEO: GSE90834 and GSE90640.

Additional resources

Yssel's Medium

Yssel's Medium is prepared in house by using IMDM (Invitrogen) plus 0.25% (w/v) bovine serum albumin (Sigma), 1.8 μg/L 2-amino ethanol, 40 μg/L Apo-transferrin, 5 μg/L insulin and penicillin/Streptomycin.

KEY RESOURCES TABLE

REAGENT or RESOURCE	SOURCE	IDENTIFIER
Antibodies		
Anti-human CD3 FITC (Clone UCHT1)	eBioscience	Cat#11-0038
Anti-human CD3 BUV737 (Clone UCHT1)	BD Bioscience	Cat#564307
Anti-human CD4 FITC (Clone OKT4)	eBioscience	Cat#11-0048
Anti-human CD5 FITC (Clone UCHT2)	eBioscience	Cat#11-0059
Anti-human alpha beta TCR FITC (Clone IP26)	eBioscience	Cat#11-9986
Anti-human gamma delta TCR FITC (Clone B1.1)	eBioscience	Cat#11-9959
Anti-human CD14 FITC (Clone TÜK4)	Miltenyi Biotec	Cat#130-080-701
Anti-human CD19 FITC (Clone LT19)	Miltenyi Biotec	Cat#130-104-650
Anti-human CD7 PE-CF594 (Clone M-T701)	BD Bioscience	Cat#562541
Anti-human CD56 AF700 (Clone B159)	BD Bioscience	Cat#557919
Anti-human CD127 PE-Cyanine 7 (Clone eBioRDR5)	eBioscience	Cat#25-1278
Anti-human CRTh2-PE (Clone BM16)	Miltenyi Biotec	Cat#130-098-238
Anti-human CD294 (CRTh2) Alexa Fluor 647 (Clone BM16)	BD Bioscience	Cat#558042
Anti-human CD117 BV605 (Clone 104D2)	Biolegend	Cat#313218
Anti-human NKp44 BB15/AF647 (Clone p44-8)	BD Bioscience	Cat#565099/558564
Anti-human CD45RA VioBlue (Clone T6D11)	Miltenyi Biotec	Cat#130-098-180
Anti-human CD25 eFluor450 (Clone BC96)	eBioscience	Cat#48-0259
Anti-human IL1R1 APC	R&D	Cat#MAB2692
Anti-human CD69 BV421 (Clone FN50)	Biolegend	Cat#310930
Anti-human CD196 PerCP-Cy5-5 (Clone 11A9)	BD Bioscience	Cat#560467
Anti-human CD304 BV421 (Clone 12C2)	Biolegend	Cat#354514
Anti-human EOMES PE (Clone WD1928)	eBioscience	Cat#12-4877
Anti-human T-BET BV421 (Clone 4B10)	Biolegend	Cat#644816
Anti-human/mouse GATA-3 PerCP-eFluor 710 (CloneTWAJ)	eBioscience	Cat#46-9966
Anti-human/mouse RORgamma (t) APC / PE (Clone AFKJS-9)	eBioscience	Cat#17-6988/12-6988
Anti-human/mouse PLZF PE	eBioscience	Cat#12-9320-82
Anti-human CD94 APC-Vio770 (Clone REA113)	Miltenyi Biotec	Cat#130-101-146
Anti-human IFNγ FITC (Clone 45-15)	Miltenyi Biotec	Cat#130-091-641
Anti-human IL-13 BV421 (Clone JES10-5A2)	BD Bioscience	Cat#563580
Anti-human IL-22 PE-Cyanine7 (Clone 22URTI)	eBioscience	Cat#25-7229
Anti-human IL-17A APC (Clone CZ8-23G1)	Miltenyi Biotec	Cat#130-094-519
Anti-human CD45 BV711/AF700 (Clone HI30)	BD Bioscience	Cat#564358/560566
Anti-H3K4me2 (Clone Y47)	Abcam	Cat#ab32356
Anti-human CD3 biotin (Clone OKT3)	eBioscience	Cat#13-0037-82
Anti-human CD4 biotin (Clone RPA-T4)	eBioscience	Cat#13-0049-82
Anti-human CD19 biotin (Clone HIB19)	eBioscience	Cat#13-0199-82
Anti-human CD123 biotin (Clone 6H6)	eBioscience	Cat#13-1239-82
Anti-human CD14 biotin (Clone 61D3)	eBioscience	Cat#13-0149-82
Anti-biotin MicroBeads	Miltenyi Biotec	Cat#130-090-485
CD34 MicroBead Kit	Miltenyi Biotec	Cat#130-046-702
Biological Samples		
Healthy human peripheral blood	EFS Paris	N/A

RORC mutation patients peripheral blood	Prof. JLC (Necker Medical School)	N/A
Human fetal liver	Advanced Bioscience Resources	N/A
Cord blood	EFS Paris	N/A
Human tonsil	Dr. RC & PG (Casa Sollievo della Sofferenza)	N/A
Human Lung	Dr. JMS (Hôpital Bichat)	N/A
Human Intestine	Dr. MA (Hôpital Saint Louis)	N/A
Human AB Serum	EFS Paris	N/A
Chemicals, Peptides, and Recombinant Proteins		
Human IL-2 IS, premium grade	Miltenyi Biotec	Cat#130-097-744
Human IL-7, premium grade	Miltenyi Biotec	Cat#130-095-362
Human IL-12, premium grade	Miltenyi Biotec	Cat#130-096-704
Human IL-18	MBL International	Cat#B001-5
recombinant human IL-17E/IL-25	R&D	Cat#1258-IL
recombinant human IL-33	R&D	Cat#3625-IL
recombinant human IL-1β	R&D	Cat#201-IL
recombinant human IL-23	R&D	Cat#1290-IL
Phorbol 12-Myristate 13-acetate (PMA)	Sigma-Aldrich	Cat#P-8139
Ionomycin	Sigma-Aldrich	Cat#I0634
BD GolgiPlug Protein Transport Inhibitor	BD Bioscience	Cat#555029
Formaldehyde	Sigma-Aldrich	Cat#F8775
Bovine serum albumin	Sigma-Aldrich	Cat#A-3675
2-amino ethanol	Sigma-Aldrich	Cat#E-0135
Apo-transferrin	Sigma-Aldrich	Cat#T-2252
Insulin	Sigma-Aldrich	Cat#I-5500
Isove's Modified Dulbeco's Medium (Glutamax)	ThermoFisher	Cat#31980
Critical Commercial Assays		
Foxp3/Transcription Factor Staining Buffer Set	eBioscience	Cat# 00-5521
BD Cytofix/Cytoperm Kit	BD Bioscience	Cat# 554714
Dynabeads mRNA Direct Kit	Life Technologies	Cat#61012
Nextera DNA Library Prep Kit	Illumina	Cat#FC-121-1030
T7 High Yield RNA Synthesis Kit	NEB	Cat#E2040S
NextSeq 500 High Output v2 Kit	Illumina	Cat#FC-404-2005
Deposited Data		
Bulk RNA Seq data	NCBI GEO	GEO: GSE90834
Chip-Seq	NCBI GEO	GEO: GSE90640
Experimental Models: Cell Lines		
Mouse: OP9	Institut Pasteur	Cat#CRL-2749
Mouse: OP9-DL4	Institut Pasteur	N/A
Experimental Models: Organisms/Strains		
Mouse: BRGS (**B**ALB/c **R**ag2$^{-/-}$ IL-2R**γ**c$^{-/-}$ **S**IRPα^{NOD})	Institut Pasteur	N/A
Sequence-Based Reagents		
Affinity Script	Agilent	Cat#600107
Exonuclease I	NEB	Cat#M0293L
mRNA Second Strand Synthesis	NEB	Cat#E6111L

Turbo DNase I	Ambion	Cat#AM2239
RNA Fragmentation Reagent	Ambion	Cat#AM8740
T4 RNA Ligase	NEB	Cat#M0204L
Kapa Hifi	Kapa Biosystems	Cat#KK2601
dNTP	Lavorah Gmbh	Cat#NU-1005XS
Agencourt AMPure XP	Beckman Coulter	Cat#A63881
Software and Algorithms		
HOMER	(Heinz et al., 2010)	http://homer.salk.edu/homer/
BEDtools	(Quinlan and Hall, 2010)	http://bedtools.readthedocs.io/en/latest/
Bowtie2	(Langmead and Salzberg, 2012)	http://bowtie-bio.sourceforge.net/bowtie2/manual.shtml
GREAT	(McLean et al., 2010)	http://bejerano.stanford.edu/great/public/html/
DESeq2	(MI Love., 2014)	https://bioconductor.org/packages/release/bioc/html/DESeq2.html
Flow Jo_v10	FlowJo	www,flowjo.com
Prism 6	Prism-Graphpad	www.graphpad.com
Other		
Yssel's Medium	In house	N/A

Click here to download Figure CELL-D-16-02656R3_Figure1.tif

Figure 1

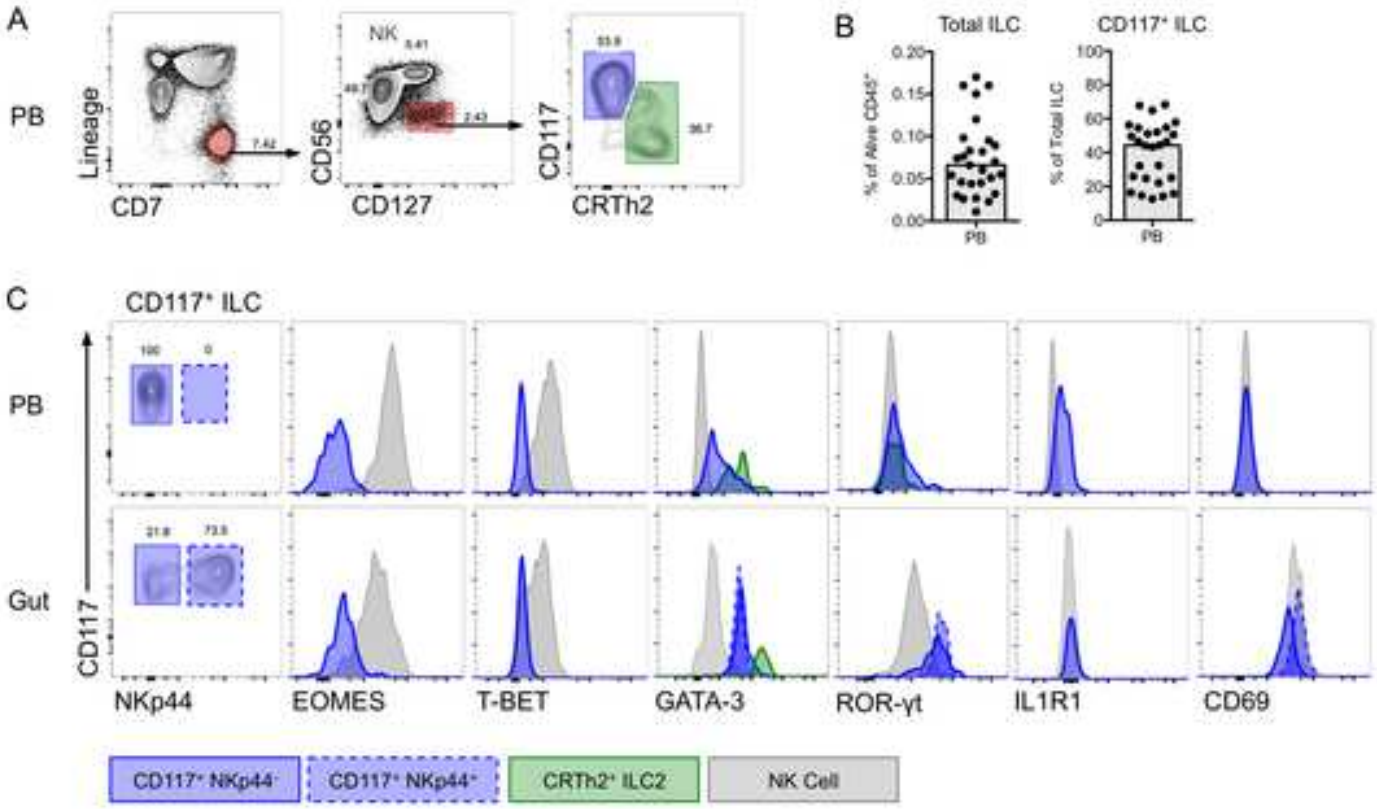

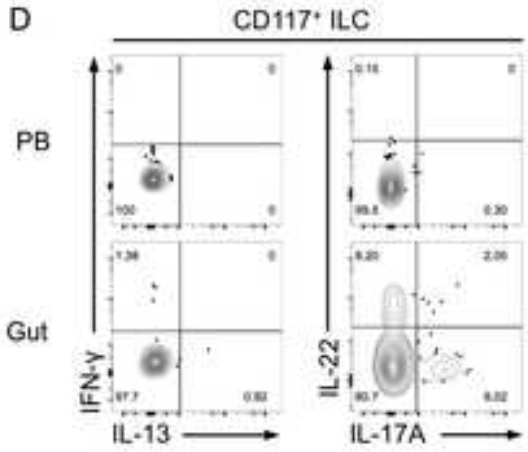

Click here to download Figure CELL-D-16-02656R3_Figure2.tif

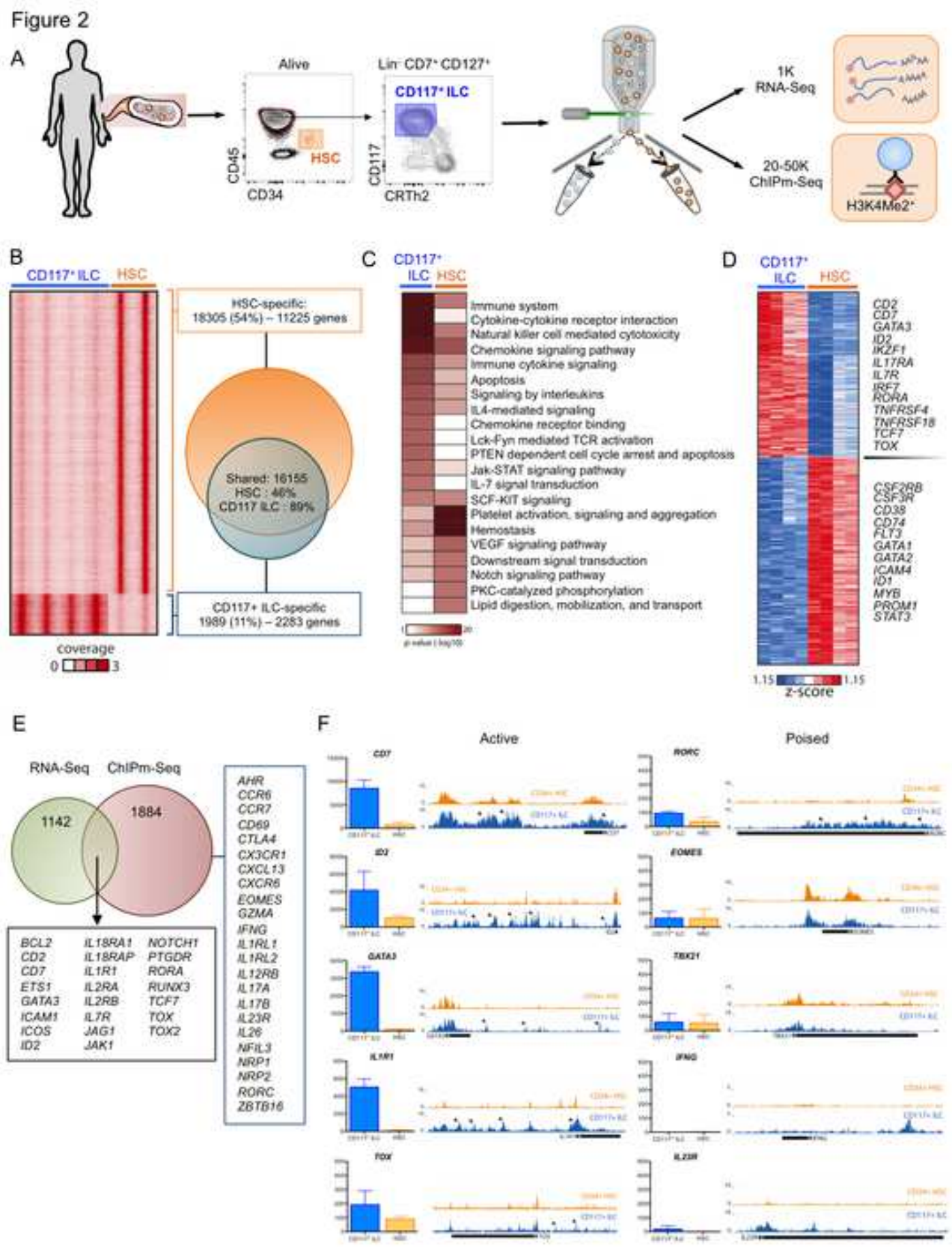

Click here to download Figure CELL-D-16-02656R3_Figure3.tif

Figure 3

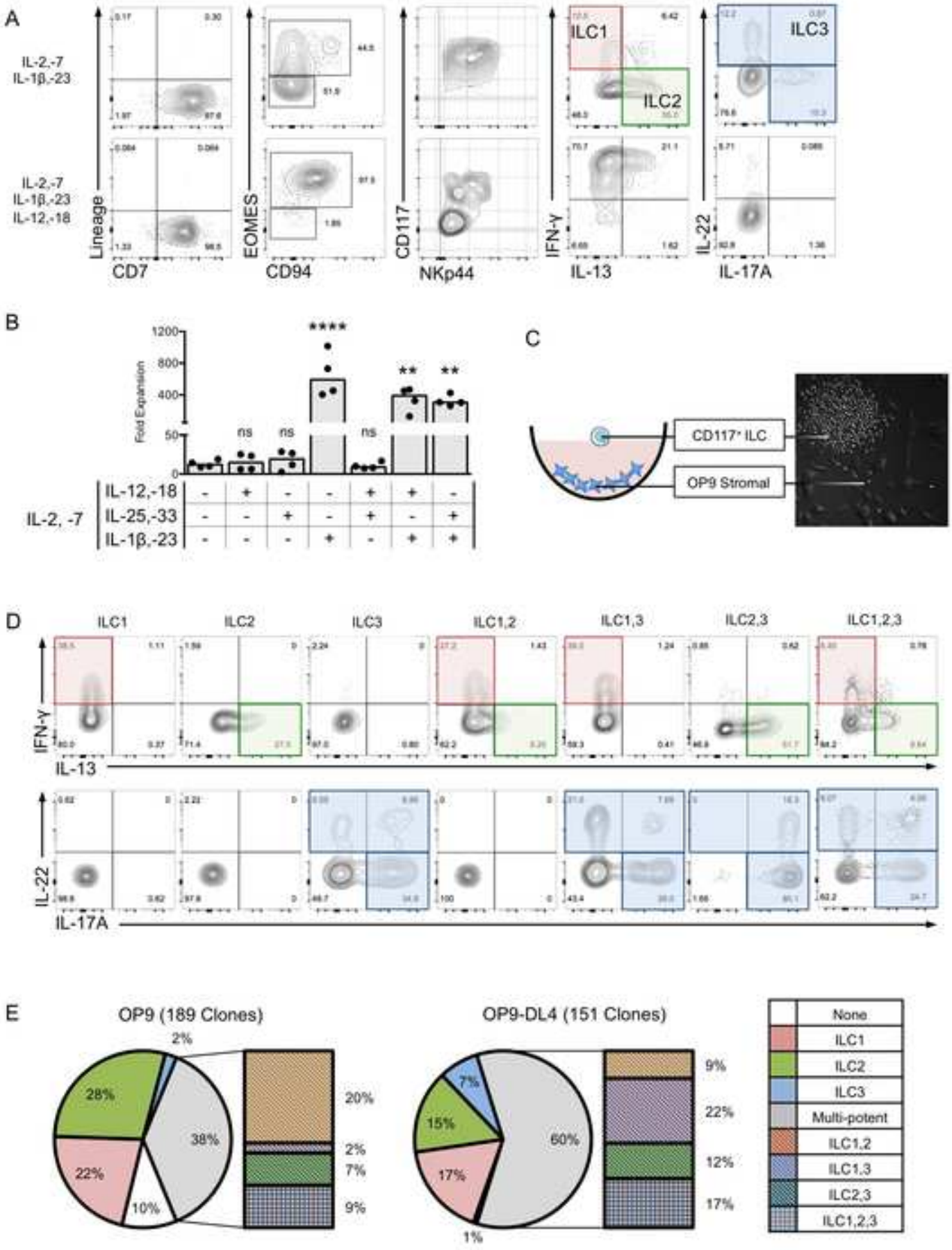

Click here to download Figure CELL-D-16-02656R3_Figure4.tif

Figure 4

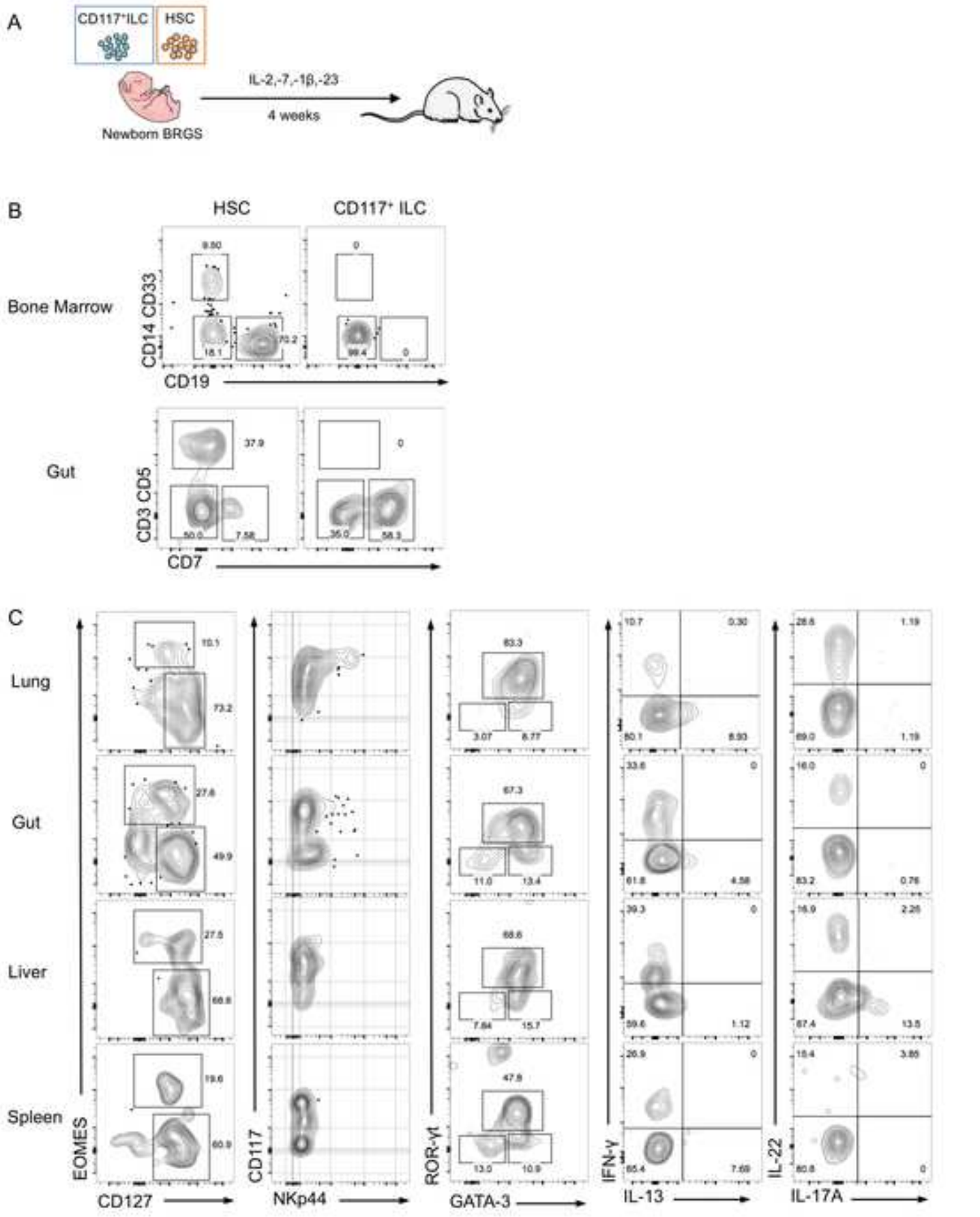

Click here to download Figure CELL-D-16-02656R3_Figure5.tif

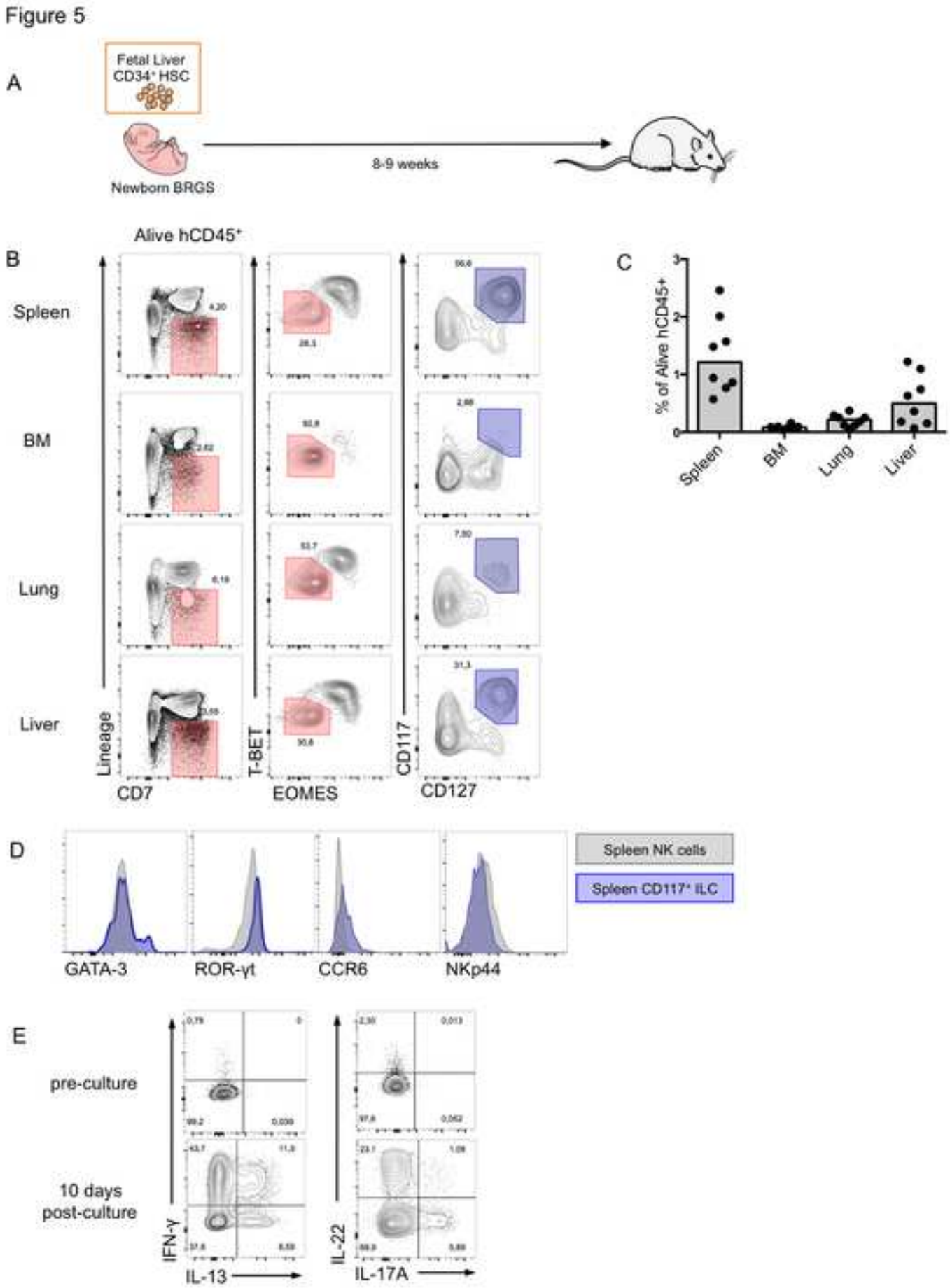

igure 6

Click here to download Figure CELL-D-16-02656R3_Figure6.tif

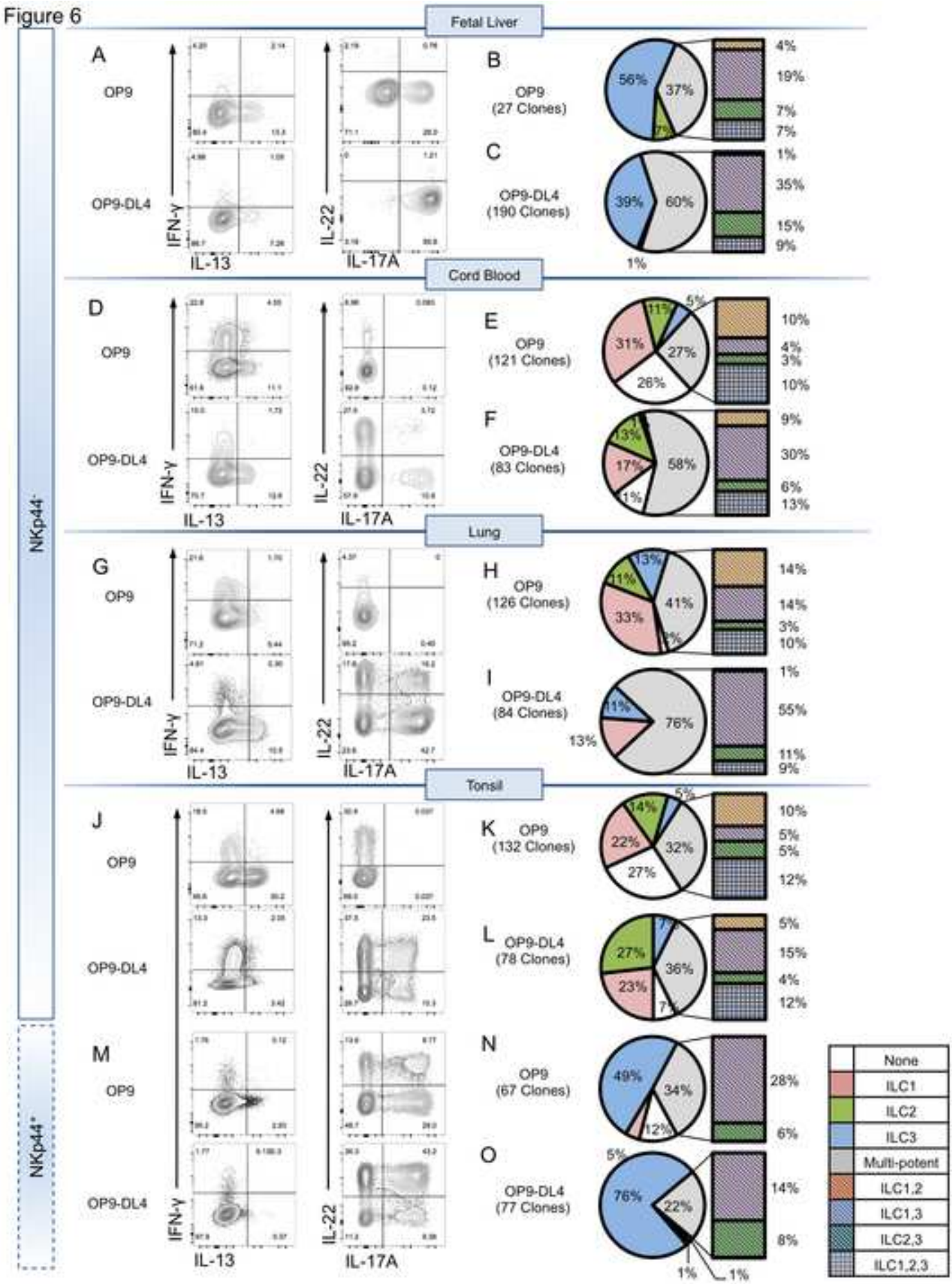

Click here to download Figure CELL-D-16-02656R3_Figure7.tif

Figure 7

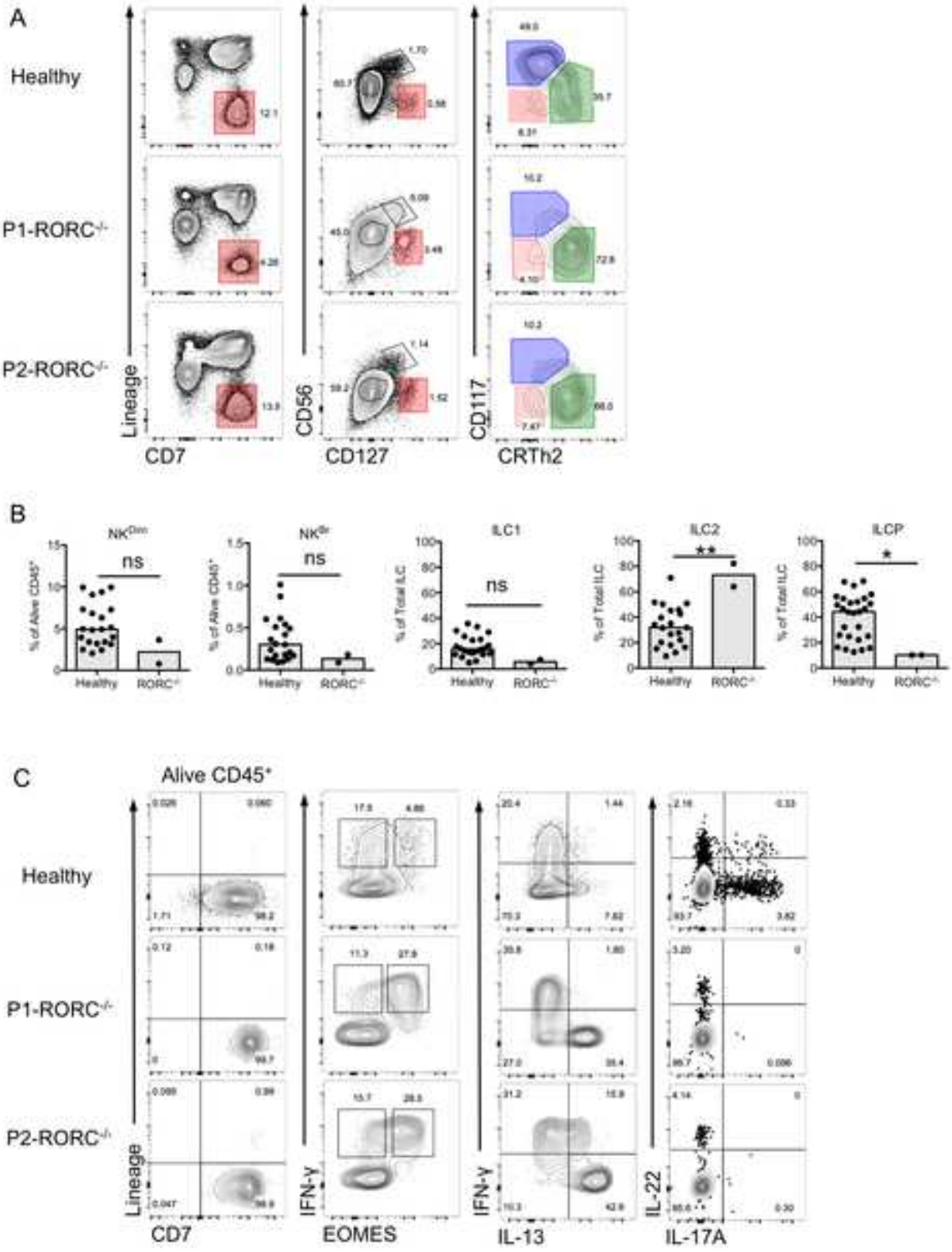

upplemental Figure 1

Click here to download Supplemental Figure CELL-D-16-02656R3_FigureS1.tif

Figure S1

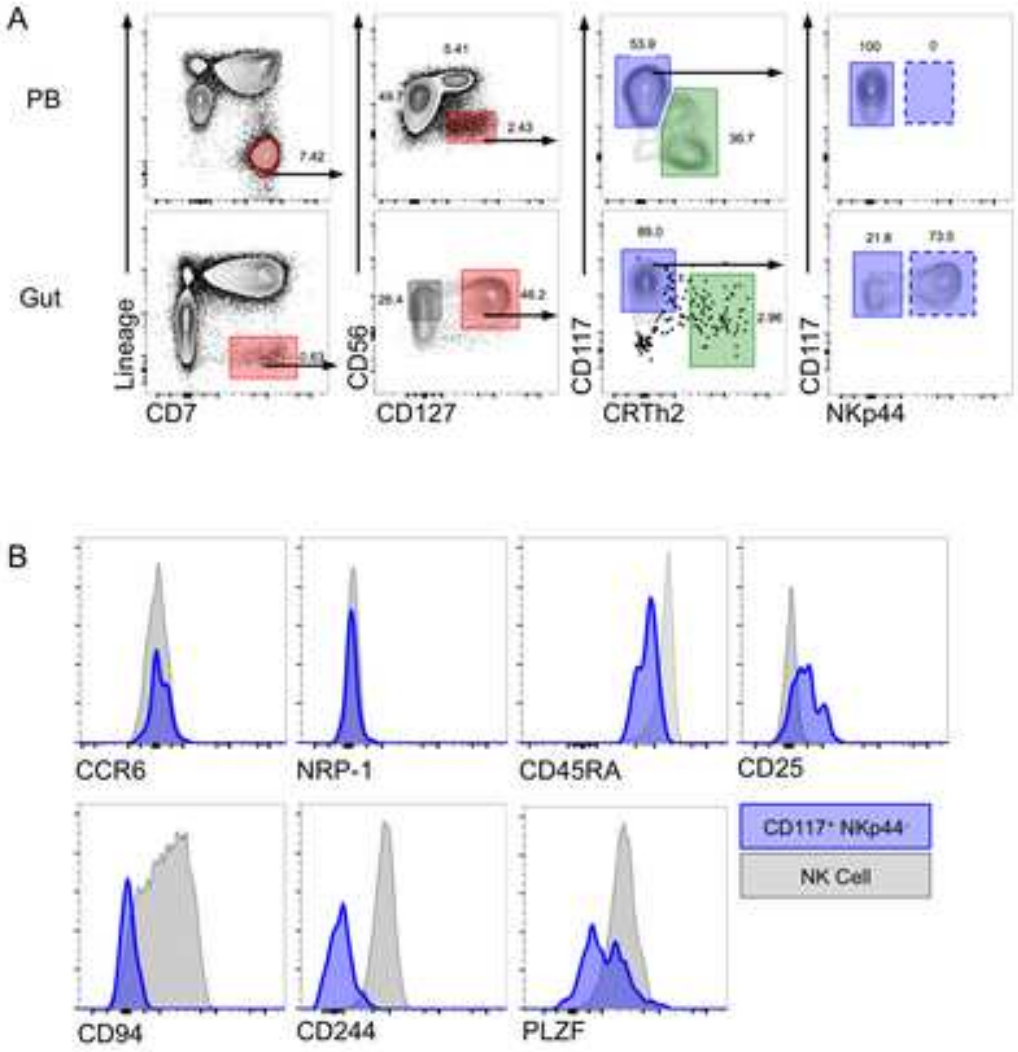

upplemental Figure 2

Click here to download Supplemental Figure CELL-D-16-02656R3_FigureS2.tif

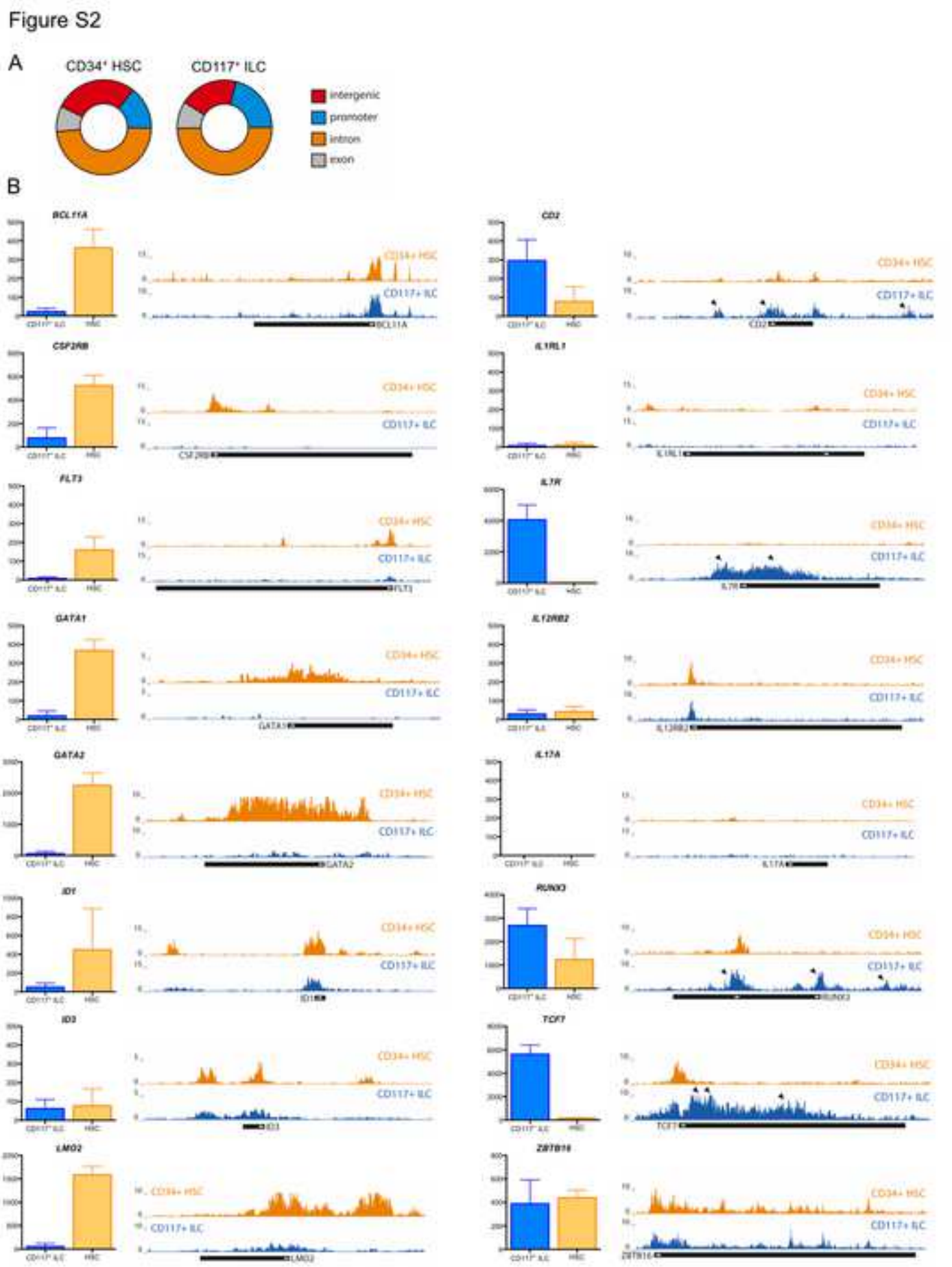

upplemental Figure 3

Click here to download Supplemental Figure CELL-D-16-02656R3_FigureS3.tif

Figure S3

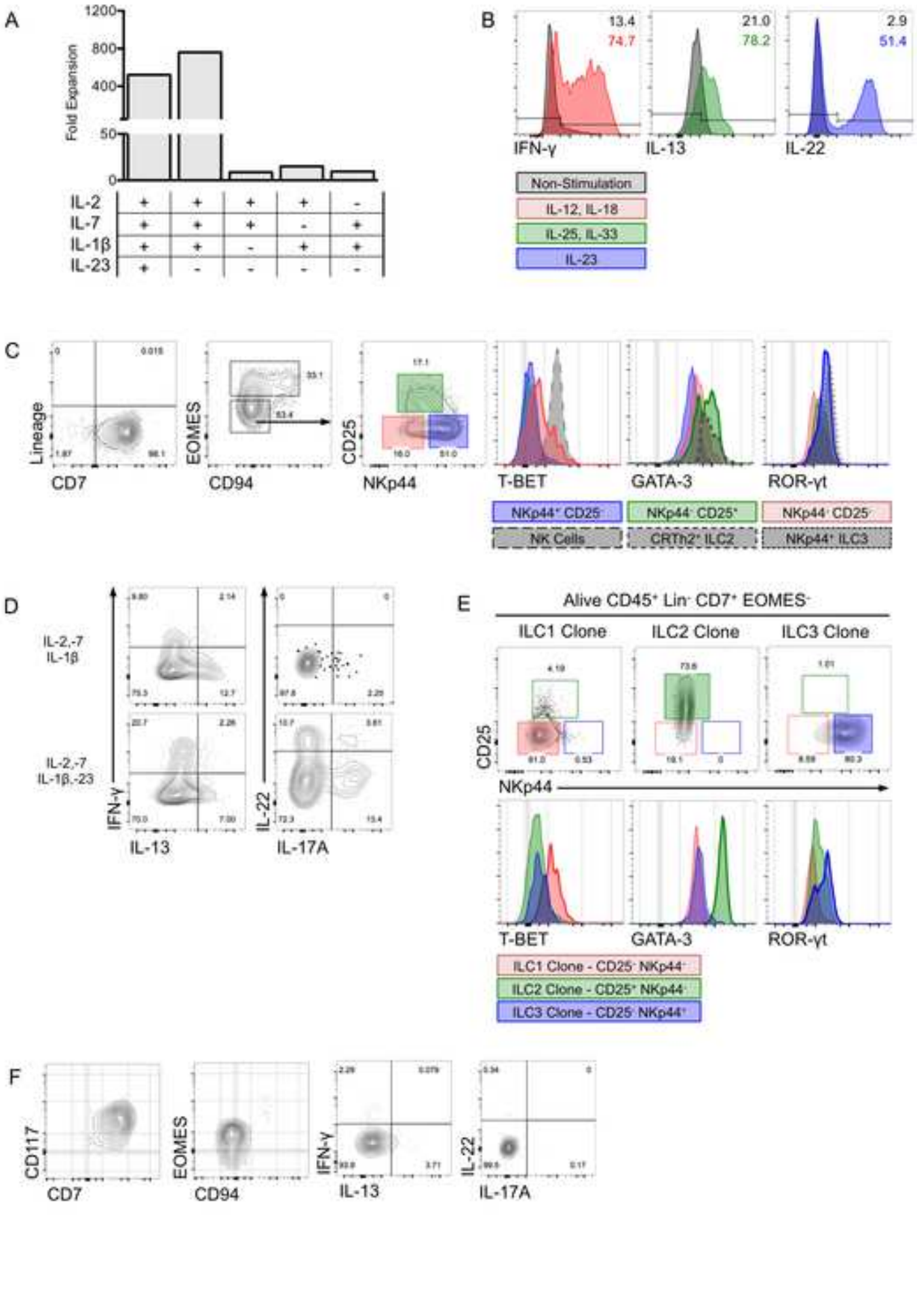

upplemental Figure 4

Click here to download Supplemental Figure CELL-D-16-02656R3_FigureS4.tif

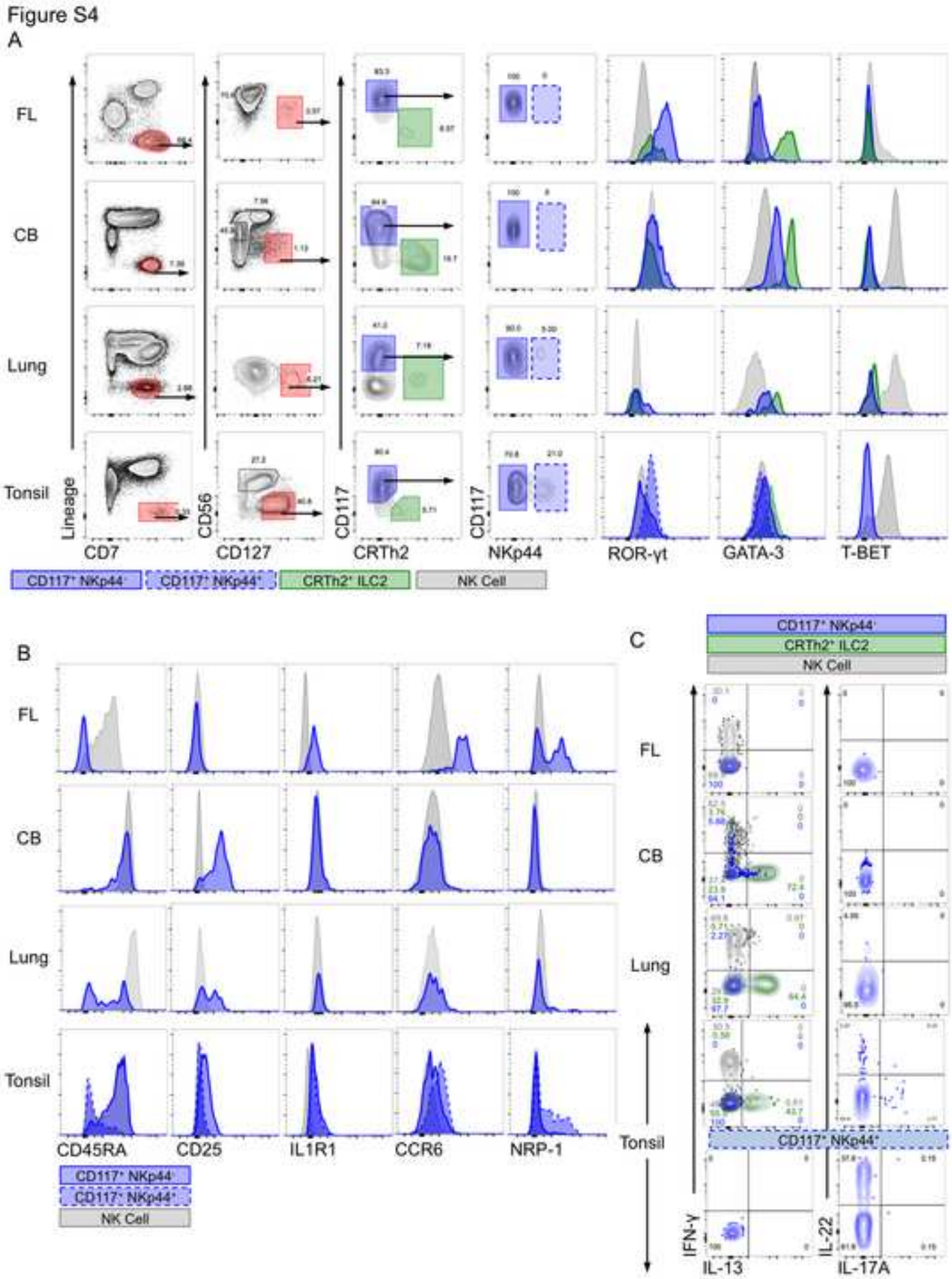

upplemental Figure 5

Click here to download Supplemental Figure CELL-D-16-02656R3_FigureS5.tif

Figure S5